Spring 2018

# Low Hemodynamic Loading Alters Heart Morphogensis in E8.5 to E9.5 Mouse Embryos

Tanner Gerard Hoog
*Missouri State University*, hoog125@live.missouristate.edu

# LOW HEMODYNAMIC LOADING ALTERS HEART MORPHOGENESIS IN E8.5 TO E9.5 MOUSE EMBRYOS

A Master's Thesis

Presented to

The Graduate College of

Missouri State University

In Partial Fulfillment

Of the Requirements for the Degree

Master of Science, Biology

By

Tanner G. Hoog

May 2018

**HEMODYNAMIC LOADING ALTERS HEART MORPHOGENESIS IN E8.5 TO E9.5 MOUSE EMBRYOS**

Biology

Missouri State University, May 2018

Master of Science

Tanner G. Hoog

## ABSTRACT

Hemodynamic loading, the force exerted on the cardiovascular walls as blood circulates, has been shown to alter heart morphology in chick and zebrafish embryos, but has yet to be shown to singly influence mouse heart development. Defects of heart morphology found in model organisms with physically altered hemodynamics resemble the aberrations seen in human congenital heart disease and are therefore crucial to understand in a mammalian model. In the present study, hemodynamic loading was altered by lowering the hematocrit of early stage mouse embryos. This was accomplished by injecting acrylamide and TEMED into the blood islands of cultured embryos to create a gel matrix which prevented blood cells from entering the circulatory system and thus created a low-hemodynamic loading environment inside the embryo's cardiovascular system. The treatment was allowed to take affect for twenty-four hours in static culture, followed by visualization using immunostaining and optical projection tomography. The embryos with lowered hemodynamic loading displayed a decrease in heart volume size and compact myocardial thickness, less defined trabeculation, and inhibition of cardiac looping. Furthermore, the results showed an unexpected outcome, whereby acrylamide-only injections of the blood islands also resulted in some morphometric heart abnormalities (trabeculation and looping). The results from this study suggest this could be due to a slight reduction in red blood cell development, indicating a continuum by which hemodynamic loading affects heart morphogenesis.

**KEYWORDS**: mouse, heart development, hemodynamic loading, trabeculation, looping

This abstract is approved as to form and content

_____

Ryan Udan, PhD
Chairperson, Advisory Committee
Missouri State University

**HEMODYNAMIC LOADING ALTERS HEART MORPHOGENESIS IN E8.5 TO E9.5 MOUSE EMBRYOS**

By

Tanner G. Hoog

A Master's Thesis
Submitted to the Graduate College
Of Missouri State University
In Partial Fulfillment of the Requirements
For the Degree of Master of Science, Biology

May 2018

Approved:

_____
Ryan Udan, PhD

_____
Christopher Lupfer, PhD

_____
Laszlo Kovacs, PhD

_____
Julie Masterson, PhD: Dean, Graduate College

## ACKNOWLEDGEMENTS

First, I would like to thank my thesis advisor, Dr. Ryan Udan, and all the wonderful people that have cycled through his laboratory, including Samantha Fredrickson, Rachel Padget, Kayla King, Bruce Green, and Shilpa Mohite. Truly, on account of these amazing people, I could not have asked to work in a better research lab.

I would also like to thank the entire MSU Biology Department for making work feel like home. Throughout my years at MSU I have had the pleasure of meeting amazing faculty and students, specifically Angeline Rodriguez who traveled through hell and back with me as we wrote our theses, Dr. Katy Frederick-Hudson whose constant optimism made every day an adventure, and of course my committee members, Dr. Laszlo Kovacs and Dr. Christopher Lupfer, for their assistance, guidance and inspiring class lectures.

My gratitude especially extends to those who assisted in this project, including members of Dr. Mary Dickinson's lab and the Optical Imaging and Vital Microscopy Core at Baylor College of Medicine. I would also like to recognize the members of the MSU Animal Vivarium, and funding supplied to this project through the TriBeta Research Grant.

Lastly, I would like to thank my friends and family who put up with my long absences and lack of communication. Thank you, to my parents for their continuous encouragement, and finally, for always being there when I needed a respite, I would like to thank by name Cameron Rudolph, Nick Rudolph, Kyle Rudolph, Christopher Filer, and Anthony Hoog.

## TABLE OF CONTENTS

## LIST OF TABLES

## LIST OF FIGURES

# INTRODUCTION

## Heart Development

Cardiovascular development is an imperative part of embryogenesis because it supplies the inner tissues of the organism with vital nutrients. In larger organisms, passive diffusion of nutrients and oxygen into the cells is limited by the overall surface area to volume ratio of the organism. For example, members of the phylum Platyhelminthes (flat worm) are limited to a flattened body which allows for passive diffusion of oxygen and nutrients (Jiang et al., 2013). Furthermore, in the phylum Nematoda, organisms can develop larger bodies due to the presence of a psuedocoelom (Atkinson, 1973), and chordates are capable of developing even larger bodies due to the presence of a closed circulatory system which efficiently supplies nutrients and removes waste from the organism's body (Pittman, 2016). Due to the necessity of the circulatory system in larger organisms, the first organ to develop during embryogenesis is therefore the heart.

In early mouse development, once the embryo has developed thick tissues, simple diffusion of oxygen and nutrients can no longer sustain the embryo and the circulatory system is therefore mandatory for the delivery of essential nutrients into deep tissue layers. At embryonic stage E6.5 (6.5 days after fertilization), heart progenitor cells are first located on the rostral portion of the epiblast before they ingress through the primitive streak and differentiate into cardiomyocytes (Tam et al., 1997). By E7.5, after ingression, the cells form two distinct sections of splanchnic lateral plate mesoderm now known as cardiogenic plates (Savolainen et al., 2009). A separate layer of endothelial cells will

eventually form ventrally to the cardiogenic plate to become the inner lining of the heart called the endocardium; however, there is much debate as to where these endothelial cell arise (Haack and Abdelilah-Seyfried, 2016). There is evidence to support their delamination from the cardiomyocytes in the cardiogenic plates (Devine et al., 2014; Ferdous et al., 2009; Misfeldt et al., 2009), but there is also evidence suggesting the endocardium is derived from vascular endothelial populations (Bussmann et al., 2007; Keegan et al., 2004; Milgrom-Hoffman et al., 2011). Despite their exact origin, endothelial cells are further specified by *Bmp* signals emanating from the *Nkx2.5* positive myocardium, and ultimately this induces the endothelium to express the endocardial-specific markers of *Nfatc1* and *Etsp71* (Ferdous et al., 2009; Palencia-Desai et al., 2015; Wong et al., 2012). In addition, *Bmp* is also required in the myocardium to produce key cardiogenic factors like *Nkx2.5* and *Mef2c* (Chen, 2004). These differentiation signals are essential to organize the right and left endocardial layers into tubes that will move medially to fuse together (Kaufman and Navaratnam, 1981). At the same time, the two cardiogenic plates (which are still continuous with the splanchnic mesoderm) will also move medially and encapsulate the endocardium. Ventrally, the cardiogenic plates will fuse, but dorsally, the splanchnic mesoderm will meet and form the dorsal mesoderm which will fuse at a slower rate. This migration pattern forms a single beating heart tube of splanchnic mesoderm-derived myocardial cells at E8.0 (Ivanovitch et al., 2017; Kelly et al., 2014).

Starting at E8.0, the heart tube, now consisting of an outer myocardial cell wall and an inner endocardium, will start to loop to the right, allowing for the positioning of the four-chambered heart to take shape (Savolainen et al., 2009). There are four stages of

cardiac looping: dextral looping, early s-looping, late s-looping, and cardiac septation (Männer, 2009). Dextral looping, or the 'c-stage' of cardiac looping, takes place during E8.0 to E8.5 and is characterized by the counterclockwise looping of the tube that makes a distinct C shape (Le Garrec et al., 2017; Männer, 2009). In order from venal to arterial, there are four prominent swellings of the tube known as the common atrial chamber, primitive left ventricle, bulbus cordis (primitive right ventricle), and the outflow tract (Kaufman and Bard, 1999). From E8.5 to E9.5 the s-looping of the heart occurs, again named after the appearance of the twisting tube which now resembles an S (Le Garrec et al., 2017; Männer, 2009). Here the bulbus cordis will shift posteriorly to develop into the right ventricle, and the common atrial chamber will move anteriorly, split into two chambers, and become the left and right atria (Kaufman and Bard, 1999; Savolainen et al., 2009). At this point the ventricles will also start to balloon and separate from one another (Anderson et al., 2006). At E10.5 the atria and ventricles are now in their correct caudal and rostral positions (Savolainen et al., 2009). To separate these chambers, the endocardium of the atrioventricular canal and the common outflow tract will undergo epithelial to mesenchymal transition to create inner wall "cushions" within the cardiac jelly found between the endocardium and myocardium (Markwald et al., 1977). These atrioventricular and outflow tract cushions will develop into the needed septal, valvular, and outflow tract structures of the adult four-chambered heart (Fananapazir and Kaufman, 1988).

Left/right gene expression plays a critical role in heart looping. For example, *Hand1* and *Hand2*, regulated by the cardiomyocyte specific gene *Nkx2.5* (Lints et al., 1993), control ventricular differentiation. *Hand1* is expressed in the left ventricle while

*Hand2* is expressed in the right ventricle (Biben and Harvey, 1997; Srivastava et al., 1997). Looping is also controlled biomechanically by means of the cytoskeletal components attached to the extra cellular matrix (Hughes and Jacobs, 2017). For example, flectin is an extracellular protein that has been found to be expressed asymmetrically around the heart tube during heart morphogenesis (Linask et al., 2003; Tsuda et al., 1996). Furthermore, if *XIN*, a gene that maintains the cytoskeleton of cardiomyocytes, or *MMP2*, which regulates the extracellular matrix around the heart, is blocked, the asymmetric cell division that drives the rightward looping of the heart ceases to initiate in chick embryos (Linask et al., 2005; Wang et al., 1999), indicating a relationship between the cytoskeletal framework and the extracellular matrix.

A more well-known biophysical force that relates to proper heart development is hemodynamic force. Blood flow begins at E8.0 when the heart is still just a simple tube, therefore all the morphological changes of the heart must develop under the continuous rhythmic process/product of systole (contraction) and diastole (relaxation). The product of these contractions is blood flow and the forces that are initiated onto the endothelial/endocardial lining of the cardiovascular system from this flow is termed hemodynamic force. This force includes both shear stress created as the blood flows over the endothelial cells (hemodynamic flow) and the pressure exerted on the endothelial wall from the mere presence of the volume. Together, shear stress and pressure are known as hemodynamic load (Midgett and Rugonyi, 2014). There is growing evidence to suggest that the main detector of hemodynamic force is primary cilia found on the apical surface of endocardial cells (Haack and Abdelilah-Seyfried, 2016; Iomini et al., 2004; Samsa et al., 2015). This type of signaling, where physical stress is conveyed into biochemical

signals, is termed mechanotransduction and can be used to initiate developmental changes of the heart (Hahn and Schwartz, 2009)

One of the morphological features of the heart that is regulated by hemodynamic force is the trabeculae. Trabeculae are projections of myocardium that extend into the lumen of the heart and are found at a higher frequency within the ventricles (Sedmera et al., 2000; Staudt et al., 2014). Trabeculae are thought to have multiple purposes: increase myocardial mass to aid in contraction, direct the flow of blood to the proceeding heart chamber, and increase surface area for oxygen absorption before and after the development of coronary circulation (Goo et al., 2009; Midgett and Rugonyi, 2014). Even though trabeculae are projections of myocardium, there is still an overlaying layer of endocardium. Studies in zebrafish have shown that the trabeculae fail to form when components of the *erbB4-erbB2* receptor complex on the myocardium, or the neuregulin ligand on the endocardium are knocked out of the organism (Gassmann et al., 1995; Lee et al., 1995; Liu et al., 2010; Meyer and Birchmeier, 1995; Morris et al., 1999; Peshkovsky et al., 2011). More recently, it has been identified that the activators of this paracrine signaling are primary cilia found on the endocardium that can respond to shear stress and activate *notch1b* (Samsa et al., 2015). The cleaved notch intracellular domain initiates neuregulin transcription, which further stimulates trabecular growth (Grego-Bessa et al., 2007; Samsa et al., 2015).

In addition to trabeculation, hemodynamic forces are also responsible for the signaling required for the formation of valves, ventricle performance, and aortic design (Combs and Yutzey, 2009; Haack and Abdelilah-Seyfried, 2016; Person et al., 2005). For example, in zebrafish, valves—endocardial leaflets that prevent reverse blood flow—are

actually induced through early retrograde blood flow which activates the valve specific transcription factor *klf2a* through *notch1b* signaling (Vermot et al., 2009). Hemodynamic stress on the outer curvature of the developing ventricle induces cells to elongate (Auman et al., 2007). Furthermore, redirection of flow during cardiac looping can cause areas of high and low stress and is responsible for the morphogenesis of symmetrical primitive left and right aortas into the single left aorta displayed in adults (Hahn and Schwartz, 2009).

Understanding the mechanisms behind heart development is essential for modern medicine. Disruptions of these innate biological processes can result in death and debilitation in the form of congenital heart disease (CHD).

**Congenital Heart Disease**

Congenital heart disease —defined as any malformation of the heart that occurs prenatally— affects approximately 5 to 10 in 1000 live births, which relates to about 1% of the population (Greutmann and Tobler, 2012; Hoffman and Kaplan, 2002; Mitchell et al., 1971). Some common examples of CHDs include abnormalities of the valves (tricuspid atresia, mitral stenosis), the ventricles (ventricular septal defect, hypoplastic left heart disease), the atria (atrial septal defect), and the aorta (aortic stenosis). Though the specific defects depend on the kind of abnormality, most lead to inefficient and/or an improperly-routed circulation. An example of a defect that causes inefficient circulation is aortic stenosis, a closing of the aorta that inhibits blood flow out of the heart (Tworetzky et al., 2004). This abnormality is usually followed by the onset of a hypoplastic left heart disease (HLHS) where blood flow is further decreased by the

presence of a small and weakened ventricle (Bardo et al., 2001). Another, and more common, form of congenital heart disease that leads to inefficient circulation is ventricular septal defects (VSD). These are hallmarked by the presence of a shunt in the ventricular septum that normally separates the right and left ventricles. When this defect is present, there is a mixing of unoxygenated and oxygenated blood, and in extreme cases (Eisenmenger syndrome) can lead to hypoxia of the entire body, also known as cyanosis (Minette and Sahn, 2006).

Though CHDs occur in 1% of live births, this frequency is an underestimation. As most CHDs form during embryonic development, these often lead to embryonic lethality, and thus go unnoticed (Hoffman, 1995). For infants with CHD that survive past the embryonic and fetal period, the most lethal time is their first year of life with 48% chance of mortality; however, if they survive past the first year, then their odds of survival dramatically increase (Gilboa et al., 2010). From 1987 to 2005, children with CHD were found to have a 66% decrease in mortality with a 96% chance of surviving to adulthood (Khairy et al., 2010). This increase in survivability is due to the invention of new surgical techniques and continuous lifetime healthcare (Greutmann and Tobler, 2012; Seal, 2011; Thakkar et al., 2017).

One of the best technologies used to circumvent CHD- related deaths, is the prenatal echocardiography which can be used to detect arrhythmias and myocardial/ventricular abnormalities *in utero* (Axt-Fliedner et al., 2006; Nelle et al., 2009). An abnormality of interest is aortic stenosis, which commonly precedes the development of hypoplastic left heart syndrome (Tworetzky et al., 2004). When aortic stenosis is detected, a surgical technique, named balloon valvuloplasty, can be conducted

at the 21-29 week stage to expand the collapsed aorta and relieve the loading inside the left ventricle (Tworetzky et al., 2004). A study in 2009 showed that this procedure was successful in developing a normal biventricular circulation 24% of the time (McElhinney et al., 2009), but its success rate has since increased to 38% as of 2014 (Freud et al., 2014).

A surgical intervention used to adapt the body to an already developed hypoplastic left heart is a three-step surgical method performed within the first year of the infant's life (Urencio et al., 2016). The first step is the Norwood procedure, where the right ventricle is manipulated into becoming the systemic circulator (Bardo et al., 2001). This is typically followed by the bidirectional Glenn and Fontan procedure to reroute the superior (Glenn) and inferior (Fontan) vena cava blood directly to the pulmonary artery for direct oxygenation of the venal blood (Norwood WI, Lang P, 1983; Urencio et al., 2016).

Ventricular septal defect treatment is determined by the degree of left ventricular overload which causes an increased ventricular preload (the blood volume present in the heart before systole). This overload is caused by the direct entrance of blood into the left ventricle from the right ventricle through the septal shunt (Minette and Sahn, 2006). If treated, an occlusion device is deployed over the shunt to prevent blood passage. This treatment was previously done through cardiopulmonary bypass (Arora et al., 2003), but more recent advances in transcatheter closure is seeing a higher success rate with minimal improvements needing to be made in the past twenty years (Arora et al., 2004; Barik, 2016). In this procedure, catheters are used to insert wires into both sides of the heart via the pulmonary artery or the femoral vein (right), and the femoral, brachial, or

axillary artery (left). On the left side, the wire is used as a guide to position an Amplazter device into the VSD. The Amplazter device is a two-part instrument that can be collapsed for passage into the heart and then expanded once in the VSD. On the right side, a proximal disc is placed on the other side the Amplazter device and sewn into place to seal the shunt. This entire procedure is done using echocardiography to visualize the process (Arora et al., 2004).

These preventive and correctional techniques are an important breakthrough for survival of these patients; however, better healthcare for fetuses and children is resulting in a growing population of adults with CHDs, now affecting about 0.5% of individuals older than eighteen (Marelli et al., 2007; Seal, 2011). Furthermore, since 1987, the deaths associated with CHD has also shifted from childhood to adulthood (Khairy et al., 2010).

While congenital heart disease has shown a major decrease in the cause of mortality (Gilboa et al., 2010), it is still a major cause of adult cardiovascular complications and even premature death (Greutmann and Tobler, 2012). Some of these complications are atrial tachycardias, which causes rapid and irregular heartbeats (Ávila et al., 2017), and heart failure due to less efficient blood flow (Nandi et al., 2017). Pregnant women with CHD have an even higher chance of developing these complications (Balci et al., 2014; Vitarelli and Capotosto, 2011). There is an estimated one million adults in the United States living with the effects of congenital heart disease and this number is predicted to grow as more surgical corrections become available (Thakkar et al., 2017).

Many CHDs have surgical solutions to them; however, the precise source of the problem continues to elude the scientific community and therefore warrants further

investigation. Through animal model studies, molecular approaches to fixing CHD *in utero* can become an option. Some of these potential therapeutic approaches include stem cell therapy to regenerate missing tissues (Wehman et al., 2015), pyruvate dehydrogenase kinase (PDK) inhibition to rescue the Krebs cycle in the myocardium (Piao et al., 2010), folic acid supplementation to stabilize the effects of accumulated reactive oxygen species (Iacobazzi et al., 2016; Qipshidze et al., 2012), and new ways of detecting CHDs can be accomplished by monitoring abnormal placental mRNAs in the maternal blood stream (Curti et al., 2016). A more sophisticated approach to molecularly correcting CHD development might lie in genome editing. In a recent study, Carroll and colleagues were able to utilize the CRISPR/Cas9 system to induce knockdowns of specific genes in mouse cardiomyocytes to produce alterations in heart morphology *in utero* (Carroll et al., 2016). To utilize these tools for human medicine, we must first understand how congenital heart diseases arise, and the best way to do that is through studies with animal models.

**Causations of Altered Heart Morphology**

Many studies in humans and animal models have revealed that the causes of CHDs are complex and can be related to genetic, teratogenic and biophysical factors. In humans, revealing the genetic cause can be done by genetic screening within affected families, and associating the CHD with specific genetic loci. This results in the identification of candidate genes involved in CHD formation. However, some loci result in mutations involving large DNA fragments. For example, about 5% of all CHD patients have large chromosomal deletions (DiGeorge syndrome) or duplications (Down

syndrome) (Digilio and Marino, 2016). While these types of studies are helpful in identifying candidate genes related to CHD, this information does not always link a specific phenotype to a genotype. Using specific genetic animal knockout models, researchers have been able to identify specific genes related to CHD. Some of these genes, namely *Nkx2.5, Gata4, Tbx5, Zic3, Tfap2b, Tbx1,* and *Fog2,* encode transcription factors that are active in the heart (Clark et al., 2006). Others are heart contractility genes like *Myl7/Mlc2a, Ncx1, Tnnt2,* and *Myh7* (Granados-Riveron and Brook, 2012) and shear stress responsive genes, such as *Nos3* and *Klf2* (Groenendijk et al., 2007).

*NKX2.5* is known as a major determinant of heart development (Lints et al., 1993; Lyons et al., 1995) and since it was linked to CHD in 1998 (Schott et al., 1998), many *Nkx2.5* knockout studies performed in mice have identified several morphological pathways regulated by this gene (Prendiville et al., 2014). For example, *Nkx2.5* knockouts disrupt *Hand1* expression and cause looping abnormalities (Tanaka et al., 1999). When *Nkx2.5* is conditionally knocked-out in the left ventricle, *Bmp10* is overly expressed and leads to increased trabeculation (Pashmforoush et al., 2004; Schott et al., 1998). Another gene regulated by *Nkx2.5* is the *Mlc2v* gene which is involved in heart contractility (Tanaka et al., 1999).

An isoform of *Mlc2v* is *Mlc2a* (also known as *Myl7* encoding myosin light chain) and is specific to the atrium. *Myl7* mutants display deficient atrium contraction, decreased ventricular myocardial thickness, and underdeveloped trabeculae (Huang, 2003). This is also seen in zebrafish that lack the myosin heavy chain (*myh6*) (Berdougo et al., 2003) indicating cross-species similarities. This information can be directly related to CHD because studies in atrial septal defect patients have found that heart contractility genes

*MYL2, MYL3, MYH7, TNNT1* and *TNNT3* are downregulated in these patients (Wang et al., 2016).

Increased myocardium and underdeveloped trabeculae are abnormalities which commonly occur in CHD patients and, therefore, provide a link between potential gene targets and CHD development. However, It is becoming clear that single gene mutations and chromosomal deletions only explain about 25% of CHDs (Russell et al., 2018). Another important factor to consider is environmental teratogens. A teratogen is any environmental factor that leads to abnormal development of an embryo. While heart teratogens are not as extensively studied as genetic causes of CHD (Lage et al., 2012), some of the known CHD causing teratogens are maternal diseases (influenza and rubella), therapeutic drugs (ibuprofen, thalidomide) (Jenkins et al., 2007), smoking (Gianicolo et al., 2010), alcohol consumption (Karunamuni et al., 2014; Shi et al., 2017), high levels of retinoic acid (Gorini et al., 2014; Lage et al., 2012), and commonly encountered environmental contaminants like phthalates (PVC flooring) and alkylphenolic compounds (detergents) (Wang et al., 2013). A specific example of a CHD teratogen which attracted considerable scientific interest is trichloroethylene.

Trichloroethylene is a known industrial contaminant that can enter human drinking water (Vogel and McCarty, 1985). Recent evidence shows that chick embryos exposed to this teratogen exhibit ventricular hypertrophy and hatchlings have an abnormally high, 38% chance, of having a ventricular septal defect (Rufer et al., 2009). Additionally, trichloroethylene has also been shown to disrupt calcium homeostasis regulation necessary for cardiomyocyte function, leading to contractility issues that result

in altered hemodynamic flow as evidenced by under-expression of shear stress responsive genes *Klf2* and *Nos3* (Makwana et al., 2010).

Taken together, the genetic and teratogenic experiments described above share a common thread in that the effects of altered hemodynamic force, generated through contractility abnormalities, are indistinguishable from the effects of genetic mutation or chemical exposure singly. Furthermore, *Dll4* knockout mice display a collapsed aorta which can perturb flow (Anderson et al., 2015), and hypoglycemia (resulting from a diabetic mother) can decrease the embryonic heart rate (Smoak, 2002). Again, in both cases, heart abnormalities such as a smaller overall heart, thickened compact myocardium, and looping defects are exhibited, but these defects cannot be assigned to the gene/teratogen or to the altered hemodynamics. It is therefore necessary to understand how hemodynamic force by itself is capable of regulating heart morphogenesis. Several embryo manipulation studies in chick and zebrafish have attempted to disconnect genetic and teratogenic effects from those caused by alterations to hemodynamic force itself.

In zebrafish, methods for altering hemodynamic load include glass bead insertion surgeries (Hove et al., 2003) and centrifugation (Johnson et al., 2015). In the glass bead surgeries, the bead can be placed at the outflow tract (high load), or at the mouth of the atrium (low load) to keep blood from exiting or entering the heart respectively. In both cases, the bulbous (outflow portion of the three chambered fish heart) and atrioventricular valves fail to develop, and the heart does not loop (Hove et al., 2003)

In chicks, which exhibit a four-chambered heart, similar to that in humans, methods for altering hemodynamics include ligations of certain parts of the cardiovascular system to perturb blood flow. Left atrial ligation which perturbs blood

flow into the left ventricle, creates a low load environment in the left ventricle and a high load environment in the right ventricle. Outflow tract ligation prevents blood from leaving the left ventricle and creates a high load in the left ventricle. Vitelline vein ligation prevents blood from entering the right atrium and creates a heart-wide low loading affect (Midgett and Rugonyi, 2014). When the vitelline vein of chick embryos is ligated, the blood flow in the heart is disturbed and leads to unorganized endocardial cell arrangement; whereas in normal embryos, the endocardial cells arrange to the direction of flow. Furthermore, the ventricular myocardium has a reduced size and the trabeculation is reduced (Hogers et al., 1997; Midgett and Rugonyi, 2014). When right (left atrial ligation) and left (outflow tract ligation) ventricles undergo increased preload, compact myocardium switches to a hypertrophic state and trabeculae become spiraled and compacted to compensate for the increased pressure (Midgett and Rugonyi, 2014; Sedmera et al., 1999).

These studies conclude that hemodynamic force plays a large role in heart morphogenesis and in turn can lead to CHD. There are obviously similarities in heart morphogenesis response to hemodynamics through different clades, as evidenced in similarities found in chick and zebrafish studies, but it is more important for medicinal reasons to see if these morphological changes are consistent in mammalian hearts. As Mahler and colleagues summarized, chick and zebrafish are easier and less costly to experiment on, but they lack placental development and high genetic similarity to humans which is why mice are more appropriate to study (Mahler and Butcher, 2011). While there have been some hemodynamic studies in mice (Anderson et al., 2015; Huang, 2003; May et al., 2004; Weissgerber et al., 2006), these are done using genetic

knockouts, and as mentioned above, the goal is to alter hemodynamics singly to rule out all other possible causes of the defects. It can be assumed that mammalian hearts will respond in a similar manner to altered hemodynamics since chick and zebrafish display similar phenotypic abnormalities and they are widely separated on the tree of life. The problem with conducting these studies in mice, until now, pertained to the inability of a working methodology.

**Hypothesis and Derivation of Methodology**

Altering hemodynamic force in a mouse embryo is problematic because previous methods used on zebrafish and chicks would require surgical manipulation of the heart. Unlike fish and chicks which develop on top of their yolk sac and naturally grow outside a maternal host, mouse embryos are encased in their yolk sac and are embedded into the uterus. *In vitro* culturing of certain stages of a mouse embryo is achievable and has been done for years, but a key aspect of this technique is keeping the integrity of the yolk sac unobstructed. This prevents previously established surgical manipulations of the heart from being utilized. Therefore, for this study, a relatively novel method of reducing hematocrit (the ratio of blood cells to total volume of the blood) was used, whereby blood cells were trapped within their spot of origin (i.e. blood islands) located proximal to the ectoplacental cone of the yolk sac. When blood cells fail to enter circulation, blood flow continues as normal, but due to the lack of viscosity supplied by the blood cells, there is a systemic reduction of hemodynamic loading (Lucitti et al., 2007).

With this methodology in hand, a hypothesis can now be tested determining how low hemodynamic loading will affect mammalian heart development. Based on previous

results in zebrafish and chick embryos that were forced to undergo reduced hemodynamic loading through surgical intervention, I hypothesize that the mouse heart will respond to altered hemodynamic flow in the same way: reduced myocardium, poorly developed trabecula, and overall less heart growth/development (volume and looping).

# MATERIALS AND METHODS

## Mouse Care

Mice were housed in the Missouri State University Temple Hall vivarium following National Institute of Health (NIH) guidelines. Mice were kept in a standard Ancare mouse cage and fed Purina Labdiet 5001 in accordance with the Missouri State Institutional Animal Care and Use Committee (IACUC) protocol #15-008.0-A (approved on November 20, 2014). Timed dissections were set up by placing a male and female into a new cage and fed Purina Labdiet 5008 as permitted by IACUC protocol #15-004.0-A (approved on December 01, 2014). All mice were kept at 20-23˚C under a diurnal cycle starting at 7 a.m. with 12 hours of light followed by 12 hours of dark.

Mice used in this study were of the CD1 strain and were either homozygous (*Myl7*+/+) or heterozygous (*Myl7*+/-) for the myosin light chain gene involved in heart contractility. To obtain myosin light chain mutants (*Myl7*-/-), an E10.5 lethal mutation, two heterozygous mice were bred resulting in a Mendelian ratio of affected embryos.

Mouse genotyping was performed using DNA extracted from the tip of weaned mice tails. Dissection scissors were doused in 70% ethanol and then used to clip 1-2mm off the tip of the tail. The tail cuts were treated with protease K (Thermoscientific, REF #EO0491) overnight at 55˚C in tail buffer (0.1M NaCl, 0.05M Tris, 0.1M EDTA, 5ml 10% SDS). A 1:1 ratio of phenol-chloroform (Fisher Scientific, BP17531-00) was used to separate the digested proteins from the DNA, followed by DNA precipitation with isopropanol and salt removal with 70% ethanol.

Mouse DNA was then amplified using polymerase chain reaction (PCR). Two sets of primers were used to amplify the presence of both the wild type and mutant form of *Myl7*: *Myl7* wild-type forward primer 5'-GGCACGATCACTC-3'; *Myl7* wild-type reverse primer 5'-ATCCCTGTTCTGG-3'; *Myl7* mutant forward primer 5'-ACAGGGAATCACA-3'; *Myl7* mutant reverse primer 5'-CGAACCTGGTCGA-3'. A 40µl reaction mixture was created using Taq Pro Red Complete (Denville Scientific Inc., CB4065-4), genomic DNA and primers. The PCR reaction was completed in a TECHNE thermocycler (3PRIMEBASE/02) set to denature at 95˚C for five minutes, followed by 35 cycles of denaturing at 95˚C for 30s, annealing for 30s at 56.5˚C, and extending at 72˚C for one minute. This cycle was concluded with a final extension period of five minutes. The amplicon was then electrophoresed through a 1% agarose gel, supplemented with 8µl of ethidium bromide, set to 100V. Visualization of the amplified product was viewed on an Azure Biosystems c300 transilluminator and digital imaging system.

**Timed Embryo Dissections**

Timed embryo dissections were set up using *Myl7*+/+ mice on a CD1 background. Embryos were dissected eight days (E8.5, somite stage 4-6) after the vaginal plug was present (E0.5). The mother was sacrificed using $CO_2$ inhalation followed by cervical dislocation. The uterus was removed from the mother and placed in a 60 mm x 15mm Petri dish (Falcon®, REF # 351008) with warm, sterile dissection media. Dissection media consisted of Dulbecco's Modified Eagle Medium (Gibco®, REF # 11330-032) with 10% fetal bovine serum (Gibco®, Cat # 10082139) and 1% penicillin/streptomycin

(Gibco®, REF # 15140-122). Individual embryos were dissected in a custom-made heater box (cardboard box surrounded by insulating material attached to a space heater), by removing the myometrium and maternal decidua but keeping the yolk sac intact. Once dissected, embryos were moved to a 37˚C incubator with 5.0% $CO_2$.

**Blood Cell Immobilization**

Glass needles were used for injection. 0.4 mm x 75 mm glass capillary tubes (Drummond Scientific CO., Cat # 1-000-800) were melted and pulled using a MicroData PMP-102 Micropipette Puller set to the manufacturers default setting SQ20: taper length of 3 mm, outer diameter of 2-20 µm, and a tip opening of 1-2 µm. Glass needles were loaded with acrylamide or TEMED using 20 µl Eppendorf GELoader® pipette tips (Cat # 022351656).

The acrylamide mixture was made using 450 µl 2x PBS, 250 µl $DiH_2O$, 250 µl 30% Bis-acrylamide (Fisher Scientific, Cat. # BP1366), 50 µl India ink (American MasterTech, REF # STIIN25), and 20 µl of 0.5 M ammonium persulfate (Thermo Scientific, CAS # 7727-54-0). The TEMED mixture consisted of 50 µl TEMED (Fisher BioReagents, CAS # 110-18-9), 50 µl 2x PBS, and 2 µl of India Ink. Both solutions were centrifuged at 17xg for one minute and subsequently filter-sterilized using a 0.45 µm nylon filter (Fisherbrand, Cat # 09-719D) to remove debris.

After dissection, embryo blood islands, located on the yolk sac adjacent to the ectoplacental cone, were injected three to four times with an acrylamide mixture using a Pico-Liter Injector (Warner Instruments, PLI-10). TEMED was then injected into the blood islands to catalyze acrylamide polymerization forming a gel matrix surrounding the

blood islands and preventing erythrocytes from entering circulation. Embryos were classified as either no injection controls (Ni), acrylamide-only injected (Ao), or acrylamide and TEMED injected (AT).

**Embryo Static Culturing and Imaging Preparation**

After injections, the embryos were moved to a Petri dish containing blood-gassed (Airgas, REF # 29-400581151-1) culture media (1 part rat serum to 11 parts dissection media) using a modified transfer pipette (tip cut off for a larger opening). Embryos were cultured for 24 hours in 37˚C.

After 24 hours, yolk sacs were checked for blood vessel remodeling. Acrylamide and TEMED treated embryos were checked for a lack of blood vessel remodeling to indicate blood flow had been successfully reduced (Lucitti et al., 2007). Acrylamide-only and no injection controls were checked for proper blood vessel remodeling to indicate normal blood flow.

Embryos were moved to a 1.5ml Eppendorf tube and fixed in 4% paraformaldehyde (Fisher Scientific, CAS # 30525-89-4) on an oscillator at room temperature for one hour. After fixation, paraformaldehyde was removed, and embryos were washed three times with 1x PBS for ten minutes each at room temperature.

To immunostain the embryonic hearts, the embryos were first blocked for one hour in serum blocking buffer (SBT) consisting of 1x PBS supplemented with 2% donkey serum (Sigma-Aldrich, Cat # D9663-10ML), and 0.8% Triton X100 (Fisher Scientific, CAS # 9002-93-1). A 1:250 dilution of Anti-Actin, α Smooth Muscle-Cy3 (sma-cy3; Sigma-Aldrich, Cat # C6198-.2ML) in SBT was used to stain the heart for

another hour. Embryos were then washed three times with PBS + 0.8% Triton X100. The embryos were then transferred to a Petri dish of PBS to remove the yolk sac and amnion, followed by storage in 1% sodium azide PBS at 4˚C.

Optical clearing of the embryos was necessary for optical projection tomography (OPT) imaging. A 1% agarose PBS solution was boiled (for homogenization), and cooled to approximately 55˚C. The embryos were inserted into the solution, sucked into a transfer pipette (tip cut off), and manually rotated- to center the embryo- until the solution solidified. Agarose embedded embryos were then cut from the transfer pipette, dehydrated with subsequent washes of 25%, 50%, 75%, and 100% ethanol-PBS solutions. Embryos were then cleared and stored in a 1:2 benzyl alcohol- benzyl benzoate (BABB; Fisher Scientific, A396-500; Acros Organics, CAS # 120-51-4) solution.

**Optical Projection Tomography Morphometric Analysis**

Optical Projection Tomography (OPT) microscopy was selected over conventional 3D imaging (confocal) due to its ability to generate high-resolution images of internal structures within the embryonic heart tube. All 3-dimensional imaging was performed at Baylor College of Medicine utilizing a custom-made OPT microscope and following previously outlined methods (Singh et al., 2015) as detailed below.

The agarose embedded embryos were shipped to Baylor in 10ml falcon tubes wrapped in aluminum foil to prevent photobleaching. Upon arrival, samples were stored at 4˚C. The agar blocks were glued to a metallic chuck and magnetically attached to the OPT rotational stage. The agarose was submerged in a glass cuvette square filled with BABB to match the index of refraction of the agar and reduce autofluorescence.

The OPT excitation laser filter was set to 531nm (green; BP 531/40 filter) and the emission filter was set to 593nm (red; BP 593/40 filter). The embryos were aligned along their vertical axes. All embryos were imaged on the same arbitrary zoom setting of 20,000 using an Optem Zoom 125 (0.75X) objective to obtain a final voxel resolution of 2.84um for each image. The embryo was raised out of the cuvette and a series of dark-field pictures were taken. The embryo was lowered back into the BABB and individual images were captured every 0.3˚ turn of the rotating stage for a total of 1,200 images per embryo. To view the entire embryo, autofluorescence was obtained using excitation light through a BP 425/26 filter and captured using a LP 473nm emission filter.

The output bin files were converted to tiff files followed by reconstruction into 3D renditions using NRecon. The 3D renditions were compiled, viewed, and analyzed using Bitplane's Imaris®.

**Volume.** The Imaris Create Surface function was used to quantify the volume of the developing hearts. Starting at the first indication of sma-cy3 staining, at every ten z intervals the interior of the heart tube was manually traced to allow an isosurface to be reconstructed (Fig. 1). The volume of the isosurface was retrieved from the Statistics tab of the Create Surface interface.

**Myocardium Thickness.** Utilizing the Imaris Oblique Slicer function, five optical sections were placed perpendicular to the lumen of the heart tube at equidistant intervals through the length of the heart (Fig. 2 A-B). On each of the five sections, four measurements were recorded using the Measurement Points function to record the distance between the exterior to the interior of the myocardium for a total of twenty

measurements per heart (Fig. 2 C-D). Measurements were evenly distributed along the perimeter of the heart tube.

**Trabeculation.** Trabeculae were quantified using the same five optical sections used for calculating the myocardial thickness. Trabeculae were parsed from the surrounding apical myocardium using Adobe Photoshop Channel Mixer function to convert red trabecular pixels to green. The resulting images had a red myocardium and underlying green trabeculae (Fig. 2 E). To normalize the amount of trabeculation to the size of the heart at each slice, a ratio of total pixilation (red and green pixels) to green pixilation was recorded per optical slice using the ImageJ plugin: Color Pixel Counter. For heavily looped hearts where optical sections traversed multiple open areas of the heart, only the lumen of progression was used in the calculations.

To assess the quality of the trabecula, trabecular indents were counted. The Imaris Create Surface function was utilized under the specification of 'automatic creation' using a surface area detail of 1μm to obtain three dimensional isosurface reconstructions of the trabecula. The indents formed from intersecting trabecular projections were counted using this isosurface.

**Heart Looping.** Ten equidistant optical sections were taken through the length of the heart. A point was placed in the center of the heart tube lumen at each section using the Measurement Point function (Fig. 2 F) for a series of connected points from inflow to outflow labeled A to J. The ends of the line (points A and J) were then aligned along the transverse plane. Using the joined ends as a vertex, the adjacent arms that dictate the degree of the angle were drawn towards points B and I to obtain an angle of the heart helix.

**Developmental Delay**

Timed dissections were set up as previously described using *Myl7*+/- parents on a CD1 background. The *Myl7*-/-, +/-, and +/+ embryos were dissected at E9.5 or E10.5 and somites were counted.

**Red Blood Cell Count**

Timed embryo dissections, injections, and culturing were conducted as described above. After culturing for twenty-four hours, embryo diameter was measured using a microscope stage micrometer. The embryo was then transferred to one milliliter of warm heparinized PB1 buffer (137mM NaCl, 20mM KCl, 20mM $KH_2PO_4$, 143mM Na2$HPO_4$-$2H_2O$, 10mM $MgCl_2$-$6H_2O$, 100mM glucose, 3.6mM sodium pyruvate, 13.2mM $CaCl_2$-$2H_2O$, 12.5µg/ml heparin) in a 35x10mm Petri dish (FALCON, REF # 351008) and the vitelline artery was severed. The still-beating heart pumped the red blood cells (RBC) into the solution aided by the presence of heparin, an anti-coagulant as shown in previous studies (Dai et al., 2004). The yolk sac was removed, and the remaining RBCs were flushed from the vessels by dipping the yolk sac in and out of the PB1 buffer. Somites were counted and the embryo was removed from the PB1 buffer. The solution of RBCs was carefully mixed by pipette before moving them to a microcentrifuge tube. Cell counts were performed on an INCYTO C-Chip hemocytometer (DHC-B02-5) following the providers instructions: cells in five of the nine large squares were counted, averaged, and multiplied by $10^4$. As embryonic red blood cells differ from those found in adults, only relatively large, rounded, nucleated cells (Dai et al., 2004) were counted.

**Statistical Analysis**

All morphometric data sets were analyzed using a one-sided t-test, with direction based on previous findings in chick (Sedmera et al., 1999) and zebrafish (Hove et al., 2003) embryos. Levene's test was conducted to prove equal variance. In cases that did not pass the Levene's test, a Welch's t-test (t-test assuming unequal variance) was used in favor of a non-parametric Mann-Whitney U test due to unequal sample sizes. Two-sided t-tests were used when analyzing developmental delay and red blood cell counts.

# RESULTS

## Rationale and Previously Published Morphometric Findings

A previous study conducted in my lab sought to determine whether low hemodynamic loaded embryos, created by injection of acrylamide and TEMED (AT) into the blood islands of cultured E8.5 mouse embryos, would result in aberrant morphology of the heart. Heart morphology in these embryos were compared to no injection control embryos (Ni) and acrylamide-only injection control embryos (Ao), because both have been previously shown to have no effect on yolk sac size, embryo turning, or blood vessel remodeling (Lucitti et al., 2007), and a qualitative assessment of our control embryos revealed a similar finding. All three types of embryos were imaged by OPT microscopy, and morphometric analysis was performed to compare heart structures. In that previous study conducted in my lab, reducing hemodynamic loading was found to have no effect on heart volume, but a significant effect on compact myocardial width. However, in this thesis study, I reviewed the previous findings, and conducted a more robust statistical analysis of these results. Further, I continued this study, and analyzed the effects of hemodynamic loading on other aspects of heart development, namely heart trabeculation and looping.

## Low Hemodynamic Loading Decreases Volume Size in E8.5 to E9.5 Embryos

It has been previously shown that increased hemodynamic preload on the left ventricle leads to a larger volume size (DeAlmeida et al., 2007). I hypothesized that the low flow environment would have the opposite effect leading to a relative decrease in

heart volume. Due to the variety of somite stages acquired during the culturing process, two somite ranges were used to compare the data: 14-16 and 17-19 (Fig. 3 A and B). To assess volume size, an isosurface of the interior lumen of the heart was constructed (see methods) and the volume was compared among the treatments (Fig 3 C-E and G-I). In low loading embryos the volume of the heart was significantly decreased compared to both Ni and Ao controls in somite range 17-19 (Fig. 3 J), but not in the earlier somite range 14-16 (Fig. 3 F).

**Low Hemodynamic Loading Results in a Decreased Compact Myocardium Width in E8.5 to E9.5 Embryos**

As the heart develops, the endocardium is in direct contact with the flow of blood. Signals from the endocardium can be relayed to the myocardium to induce proliferation, hypertrophy, and migration (Haack and Abdelilah-Seyfried, 2016; Peshkovsky et al., 2011). Optical projection tomography does not allow visualization of individual cellular growth, but growth of the compact myocardium can still be assessed by measuring the thickness of the cultured embryo's heart (Fig. 4 D-F). Twenty width measurements throughout the length of the heart were collected per individual embryo and, in both somite ranges, the low hemodynamically loaded hearts showed a significant decrease in width size (Fig. 4 G and J).

**Low Hemodynamic Loading and Acrylamide-Only Injections Alter Trabeculation in E8.5 to E9.5 Hearts**

Myocardial trabecula of the heart starts to develop as the heart begins beating at E8.0-E8.5 and has been shown to be altered in both high loading and low loading environments of chick embryo hearts (Sedmera et al., 1999). Therefore, the next step was to evaluate how the low loading environment affects trabeculation within a mouse model. First, the surface area of the trabecula was calculated on six cross-sections per heart within the three treatment types and normalized to the total myocardium (trabeculated myocardium and compact myocardium) to prevent bias based on difference in heart size. When comparing Ni to AT, low hemodynamic loaded hearts exhibited an increase in trabeculation at both somite stages (Fig. 4 H and K). Unexpectedly, the acrylamide-only controls also showed an increase in trabeculated myocardium compared to the no injection controls. Upon visual inspection of the cross-sections, the trabecula of Ni had more projections in the lumen of the heart; whereas the Ao and AT hearts displayed compacted trabecula (Fig. 4 D-F). This characteristic can also be seen when viewing the entire surface of the outer curvature of the heart (Fig. 4 A-C).

To quantify these findings, trabecular 'indents' were counted. Trabecular indents are defined as the depression that forms when adjacent trabecular projections connect. The results showed that hearts under a normal hemodynamic loading environment develop more trabecular indents at both somite stages (Fig. 4 I and L). Again, the acrylamide-only treated embryos displayed decreased numbers of trabecular indents similar to that seen in the low loading embryos. Taken together, these observations indicate that low hemodynamic loading does not stop trabecula from forming, but it does

inhibit it from forming correctly. Furthermore, acrylamide-only injections are also capable of affecting trabecula similar to the AT injected treatments.

**Low Hemodynamic Loading and Acrylamide-Only Injections Inhibit Proper Heart Tube Looping in E8.5 to E9.5 Embryos**

Despite observing defects in trabeculation in acrylamide-only embryos, the morphological assessment proceeded to gauge how hemodynamic loading affects heart tube looping. Looping is an imperative feature of mammalian heart development because this process allows the primitive ventricle to separate into left and right portions which subsequently separates the pulmonary and systemic circulations. In previous studies, heart looping has been measured by comparing the atrioventricular junction to the anteroposterior axis (Parrie et al., 2013); however, this study was performed in zebrafish which has a simplified degree of looping. Therefore, a style more fitted for three-dimensional analysis, that has been confirmed to be reliable in mice (Le Garrec et al., 2017), was used instead. The interior looping helix of the heart was manually created, the extremities of this helix were aligned to form a circular shape along the transverse plane and an angle of the transverse helix was measured using the aligned extremities as the vortex of the angle (Fig. 5 A-I). In this manner, low loaded hearts (AT) at both somite ranges were found to be in a more linear state compared to Ni controls, and Ao injections also resulted in linearized hearts closely resembling those of the AT model (Fig. 5 J-K). In summary, low hemodynamic loading prevents proper heart tube looping, but following a trend observed in the trabeculation studies, Ao injections also inhibited looping.

**Low Hemodynamic Loading Causes Developmental Delay in E8.5 to E9.5 Embryos**

To address the question of why the Ao controls had a significant effect on trabeculation and looping of the heart, the qualitative assessment of the control and experimental embryos —that cultured Ao embryos resembled Ni embryos— was revisited by quantifying somites to determine whether the embryos exhibit developmental delay. To test this, timed dissections were performed at E8.5 (somite stage 4-6) followed by blood island injections. These injections consisted of the normal injection types (Ni, Ao, and AT) but also included PBS only (Po) and TEMED only (To). After culturing for twenty-four hours, the embryos' somites were counted and compared to both the no-injection control and the PBS injection, since these should have no effect on the embryo's development. The individual injections did not significantly alter the development of the embryos as shown with an average somite count of eighteen between all treatment types including Ao (Table 1), demonstrating that all control embryos do not exhibit developmental delay. However, the low hemodynamic loaded embryos, exhibited a significant developmental delay ($p$-value = 0.001 to Ni treatment, $p$-value = 0.005 to PBS treatment) by only reaching an average somite stage of 14 (Table 1). This was an expected result, because it was previously published that the low hemodynamic loading embryos also exhibit an impairment to other aspects of development, including smaller yolk sac, impaired turning, and an inability for the vessels to remodel (Lucitti et al., 2007)

The observed developmental delay brings up another question concerning the validity of the AT model, as addition of acrylamide and TEMED could synergistically have an effect on remodeling that is independent of reduced-hemodynamic loading. To

prove that developmental delay was caused by reduced-loading, and not the synergistic action of acrylamide and TEMED, the extent of development was compared between *Myl7* mutants (*Myl7 -/-)* to wild type controls (*Myl7 wt)*. *Myl7* (also known as Mlc2a) is a protein coding gene (myosin light chain) essential for atrial contractions of the cardiac muscle of the heart (Huang, 2003). When this protein is absent (*Myl7 -/-)*, blood flow is reduced, and in these embryos, quantitative analysis of the somites revealed a significant developmental delay of *in vivo* embryos at both E9.5 and E10.5 (Table 2). Since *Myl7* mutants (genetically altered low-loading) display a similar phenotype to the AT injected embryos (physically altered low-loading), it can be concluded that the developmental delay is likely caused by reduced-loading, and not a direct effect of the AT treatment.

**Acrylamide Decreases the Number of Systemic Primitive Red Blood Cells at E9.5**

When acrylamide was injected into the blood islands of E8.5 embryos and cultured for twenty-four hours, the blood vessels of the yolk sac properly remodeled— indicating adequate levels of hemodynamic force (Lucitti et al., 2007)— and somitogenesis was unperturbed (Table 1). However, trabeculation and heart tube looping of Ao embryos more closely resembled those of the low hemodynamic loaded embryos (Fig. 4 and 5). Since the hemodynamic loading was sufficient in remodeling the yolk sac and allowing proper heart volume/myocardial thickness development, but insufficient in promoting trabeculation and heart tube looping, I wanted to address if hemodynamic force was being negatively modulated enough to exhibit some, but not all, morphological changes.

During developmental stages E8.5 to E11.5 proerythroblasts are transitioning into polychromatic erythroblasts (Dai et al., 2004; Palis, 2014), and according to a recent study, polychromatic erythroblasts in adult rats have an increased chance of becoming micronucleated- a sign of genotoxicity- when orally administered acrylamide (Yener, 2013). Furthermore, adult rats also exhibit reduced hematocrit, and their red blood cell counts are low due to osmotic fragility and oxidative stress (Ghorbel et al., 2015). Even though these studies were conducted in adult rats, the potential for acrylamide to reduce the number of red blood cells circulating within mouse embryos did not seem unjustified.

To test the hypothesis that acrylamide can reduce red blood cell numbers within E8.5-9.5 embryos, injections were performed as normal, embryos were cultured for twenty-four hours, red blood cells were collected (see methods), and then counted on a hemocytometer. Since the RBC collection method by design could not possibly collect every red blood cell found in the embryos, somite range and yolk sac diameter size of the collected embryos were first compared to make sure there were no obvious dissimilarities between levels of development that would account for further variations in RBC numbers. The average yolk sac diameter was 2.5mm and the average somite count was 16 among Ni and Ao embryos used for RBC counting (Table 3). Furthermore, there was no correlation between yolk sac size and the number of erythrocytes found within these embryos as indicated by the low R-squared values found in both Ni (-0.0499) and Ao (0.0229) (Fig. 6). Due to this lack of correlation, there should be no growth bias influencing RBC numbers in the embryos. Therefore, all of the collected embryos in the RBC assessment were used and a significant 38% decrease in red blood cells was found in the Ao treatments compared to Ni treatments (p-value = 0.010, Table 4). This decrease

in RBC could potentially explain the abnormalities of trabeculation and looping displayed in Ao embryos.

Table 1. Developmental Delay of Different Injection Types in Terms of Somite Stage. E8.5 embryos were injected with different combinations of polymerizing chemicals and somites were counted after culturing for twenty-four hours. The *p*-values are based on a two-sided t-test.

| Injection Type | n | Somite Number | *p*-value | |
|---|---|---|---|---|
| | | | To No Injection | To PBS |
| No injection | 12 | 18.3 ± 2.6 | - | 0.693 |
| PBS | 9 | 17.8 ± 0.9 | 0.693 | - |
| TEMED | 9 | 17.6 ± 1.5 | 0.479 | 0.580 |
| Acrylamide | 26 | 18.3 ± 3.7 | 0.961 | 0.742 |
| Acrylamide + TEMED | 27 | 14.4 ± 3.4 | * 0.001 | * 0.005 |

Table 2. Developmental Delay of *Myl7* Mutants in Terms of Somite Stage. Timed dissections were performed on E9.5 or E10.5 embryos, somites were counted, and embryos were genotyped. The *p*-value was based on a two-sided t-test.

| | E9.5 | | E10.5 | |
|---|---|---|---|---|
| | *Myl7 wt* | *Myl7 -/-* | *Myl7 wt* | *Myl7 -/-* |
| Somites | 23.7 ± 1.1 | 22.4 ± 1.5 | 35.4 ± 2.1 | 30.8 ± 2.3 |
| *p*-value | * 0.010 | | * <0.001 | |

Table 3. Yolk Sac and Somite Comparison of No Injection and Acrylamide-Only Injected Embryos. The yolk sac (YS) diameter and somite stage was compared between embryos that were either not injected or injected with acrylamide and cultured for twenty-four hours. The *p*-values are based a two-sided t-test.

| Injection Type | n | YS Diameter | Somites |
|---|---|---|---|
| No Injection | 18 | 2.5 ± 0.4 | 16 ± 3 |
| Acrylamide-only | 18 | 2.5 ± 0.3 | 15 ± 3 |
| *p*-value | | 0.849 | 0.186 |

Table 4. Red Blood Cell Count in No Injection and Acrylamide-Only Injected Embryos. Red blood cells were drained from cultured embryos that received the indicated treatments and counted. The *p*-values are based on a two-sided t-test.

| Injection Type | N | RBC Count |
|---|---|---|
| No Injection | 18 | 3.66e5 ± 1.54e5 |
| Acrylamide-only | 18 | 2.28e5 ± 1.48e5 |
| *p*-value | | *0.010 |

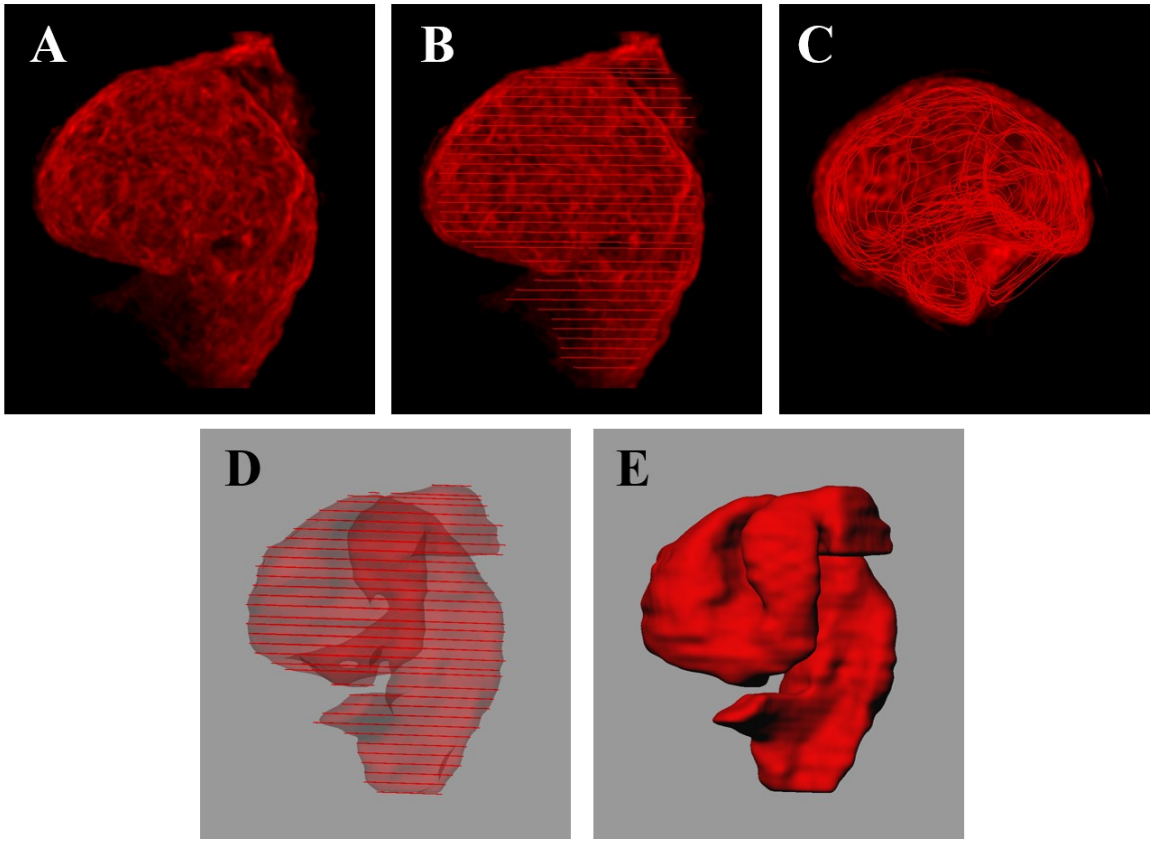


Figure 1. Isosurface Creation for Volume Comparison. The sma-cy3 fluorescence was visualized in three-dimensions and on transverse, optical cross-sections, the lumen of the heart was traced to create an isosurface. (A) Side view of the sma-cy3 fluorescence on the embryo's heart. (B) Side view and (C) dorsal view of the sma-cy3 fluorescence with layered lumen tracings. (D) Side view of the Imaris-constructed isosurface (translucent) of the heart with layered lumen tracings. (E) Imaris-constructed isosurface.

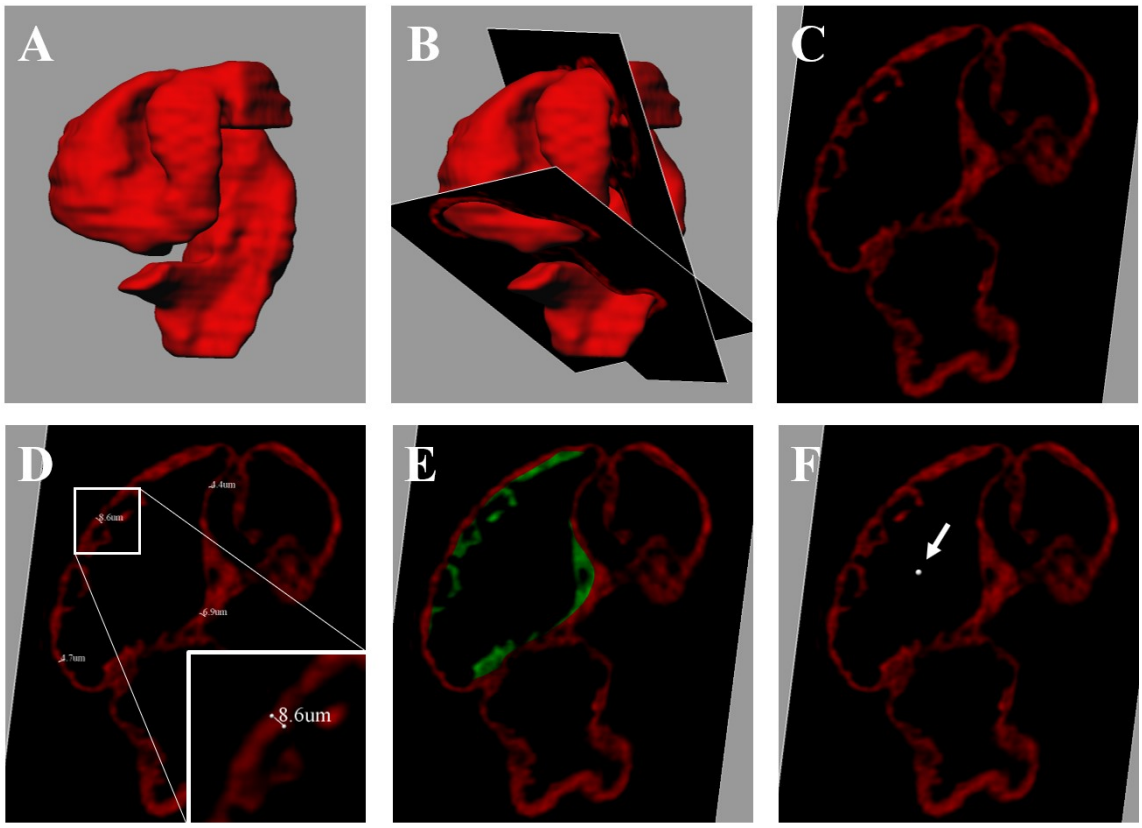


Figure 2. Method Visualization for Myocardial Thickness, Trabeculation, and Heart Looping Analysis. Optical cross-sections were placed through the length of the heart for morphometric analysis. (A) Isosurface side view of the heart. (B) Isosurface with cross-sections (only first and last cross-sections for clarity). (C) Cross-section without manipulation. (D) Cross-section with four myocardial-width measurements. (E) Cross-section with trabeculated myocardium parsed out in green. (F) Cross-section with a single point in the center of the lumen of progression (arrow points to the point), used for heart looping.

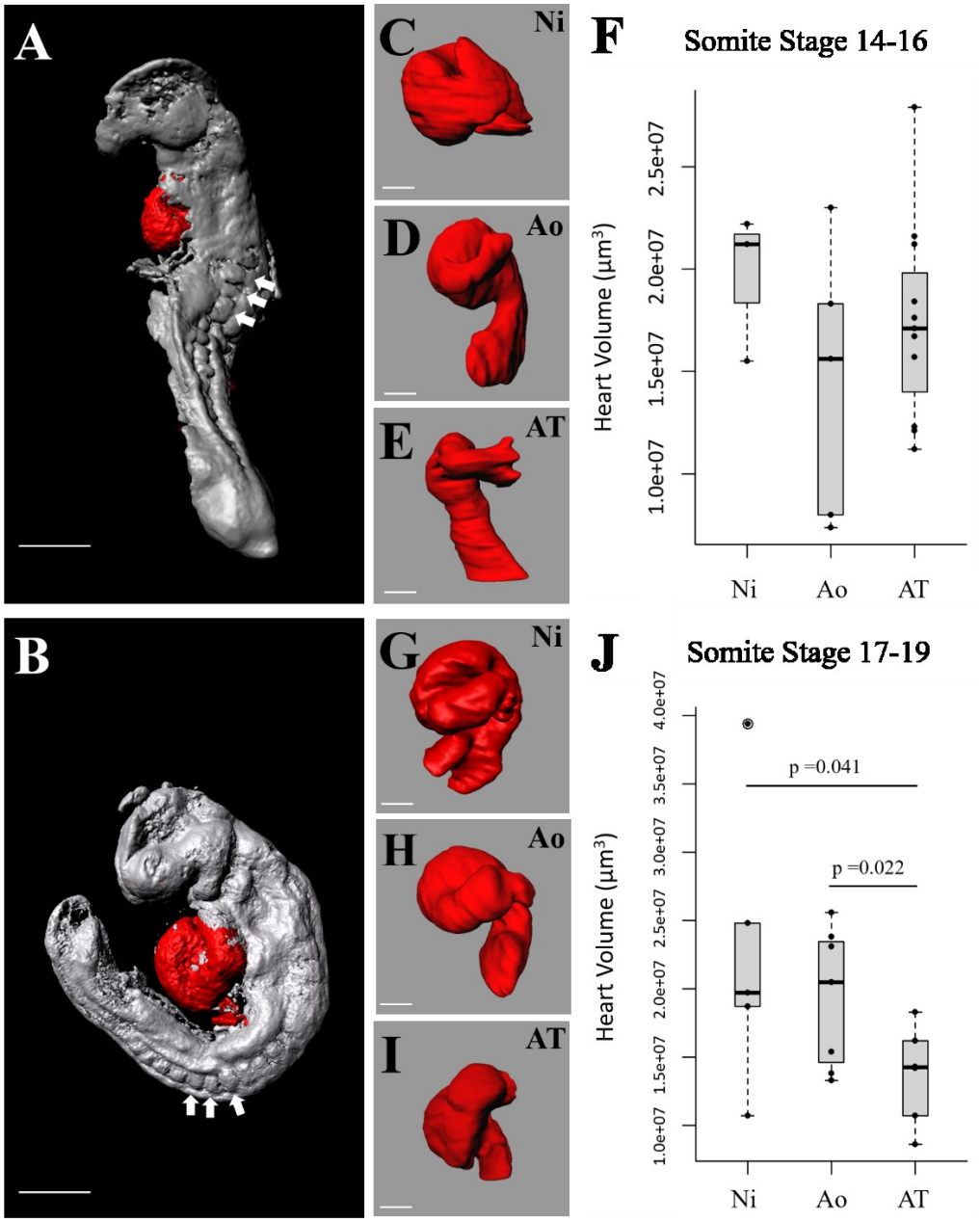


Figure 3. Isosurface and Volume Comparison of E8.5-E9.5 Mouse Hearts. Isosurfaces were created (A-B) from the autoflourescent OPT images to visualize the entire embryo, or (C-E, G-I) from the sma-cy3 immunostaining to visualize just the volume of the heart. (A-B) Representative whole embryo isosurfaces (A: Ni, somite range 14-16; B: Ni, somite range 17-19) with hearts manually colored red and somites marked with white arrows. (C-E, G-I) Representative images of whole heart volumes for somite range 14-16 (C: Ni, D: Ao, E: AT) and 17-19 (G: Ni, H: Ao, I: AT). (F, J) Boxplots of heart volume for each treatment type with indicated *p*-values based on a one-tailed t-test. A-B scale bar = 300µm; C-E, G-I scale bar = 100µm. F n= 3 (Ni), 6 (Ao), 12 (AT); J n = 5 (Ni), 8 (Ao), 7 (AT).

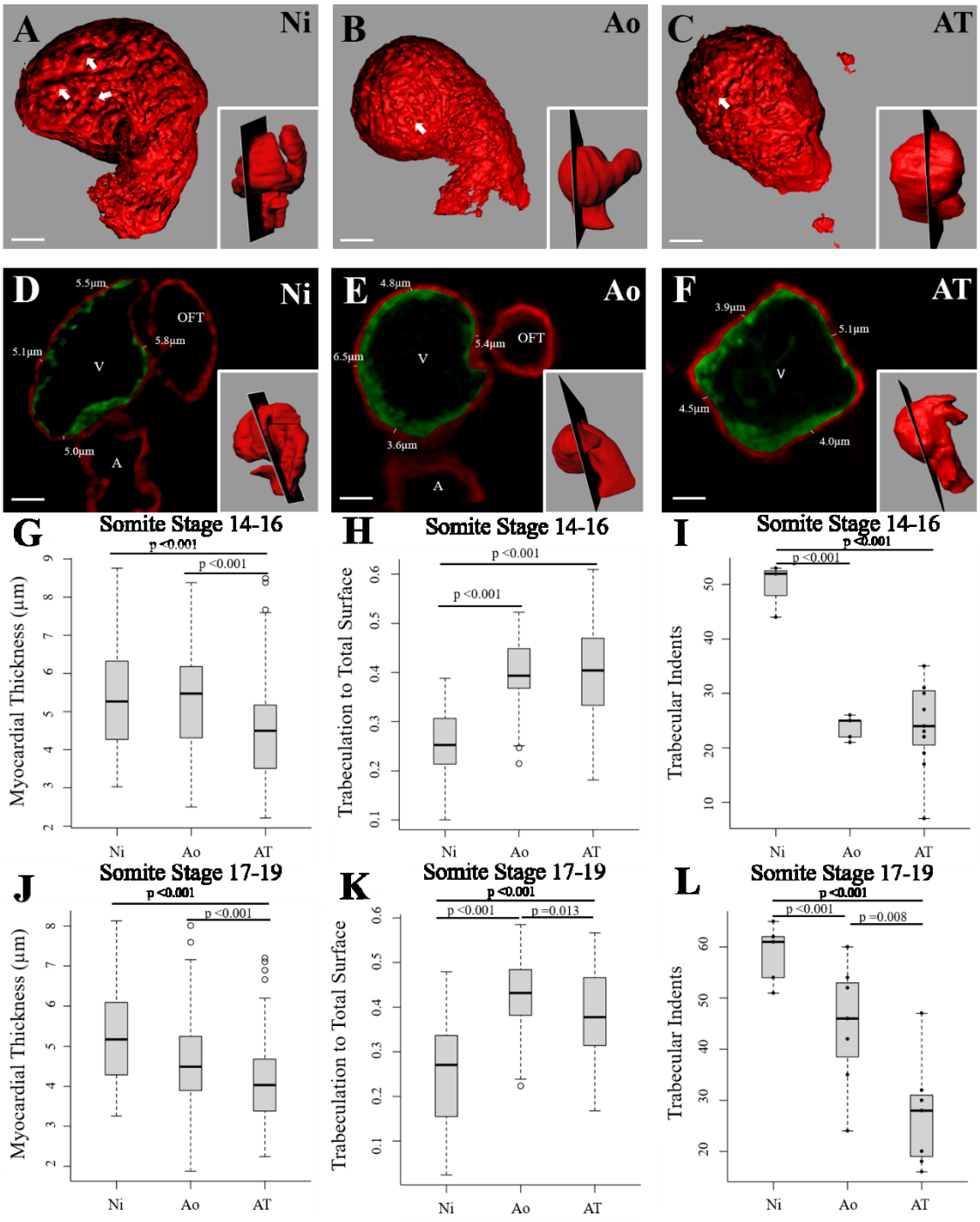


Figure 4. Myocardial Thickness and Trabeculation Comparison of E8.5 to E9.5 Mouse Hearts. (A-C) Representative images of the *en face* view of the interior lumen of the primitive ventricle with the slice position indicated by the superimposed image, and the white arrows denoting the presence of trabecular 'indents' (A: Ni, B: Ao, C: AT). (D-F) Representative optical sections of the interior lumen of the heart with the slice position indicated by the superimposed image, measured compact myocardium is labeled red, and the trabeculated myocardium is labeled green; A = Atrium, V = Ventricle, OFT =

Outflow Tract (D: Ni, E: Ao, F: AT). (G-L) Boxplots and indicated p-values for myocardial thickness (G, J), trabeculated area (H, K), and trabecular indents (I, L). The *p*-values were obtained using a Welch's t-test (G, J) and a one-sided t-test (H-I, K-L). A-F scale bar = 70µm. G-I n= 3 (Ni), 6 (Ao), 12 (AT); J-L n = 5 (Ni), 8 (Ao), 7 (AT). Myocardial thickness used 20 (n x 20) measurements per heart, and trabeculation to total surface tests used six measurements per heart (n x 6).

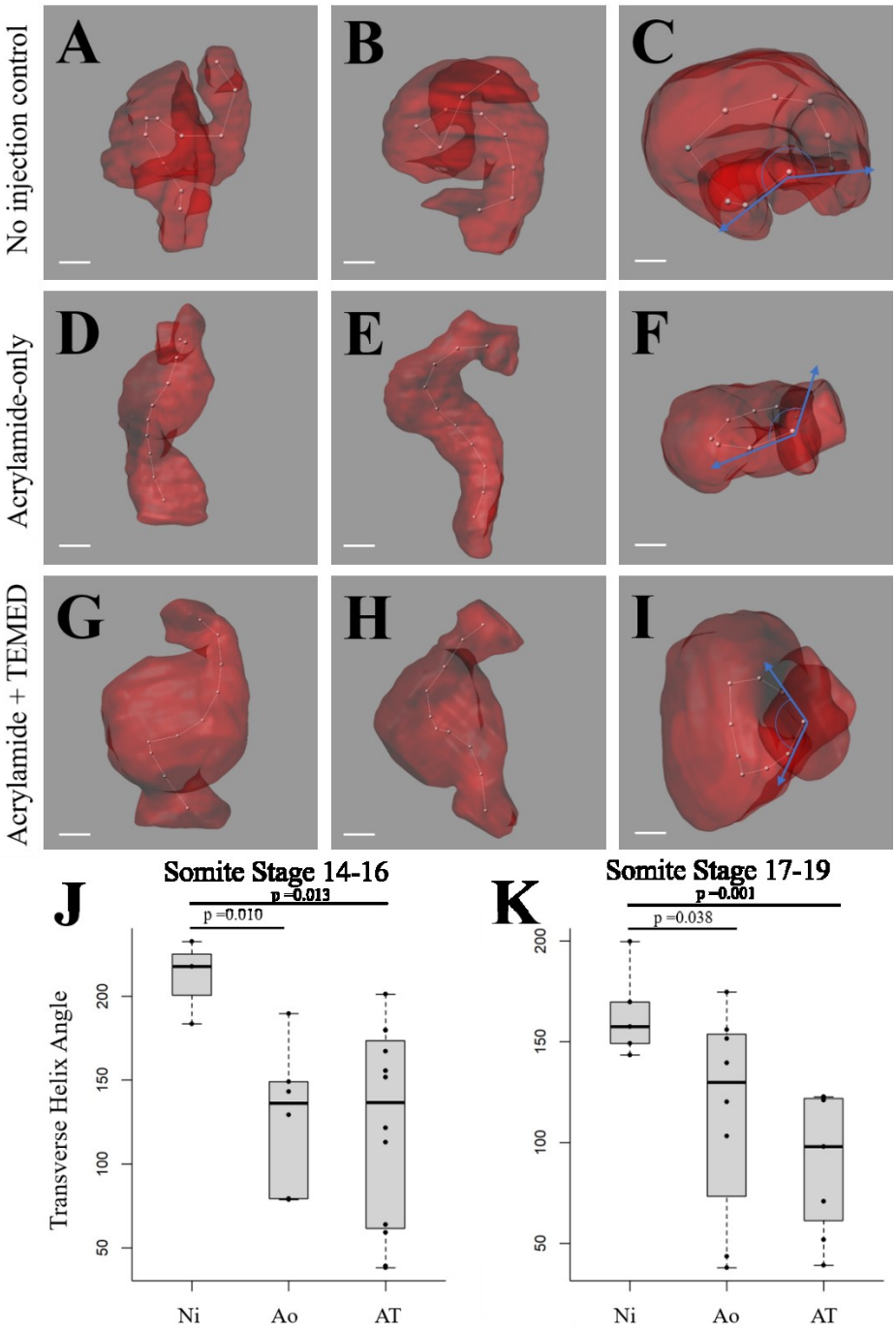


Figure 5. Heart Tube Looping Comparison of E8.5 to E9.5 Embryos. A-I Isosurface reconstructions of the heart tube with interior looping helix shown as a series of ten equidistant connected dots; A-C: Ni, D-F: Ao, G-I: AT. (A, D, G) ventral view. (B, E, H) left view. (C, F, I) Show the anterior view of the heart with the transverse helix angle overlying the aligned helix extremities. (J, K) Boxplots of the calculated transverse angles and indicated *p*-values based on a one-sided t-test. Scale bar = 70µm. J n= 3 (Ni), 6 (Ao), 12 (AT); K n = 5 (Ni), 8 (Ao), 7 (AT).

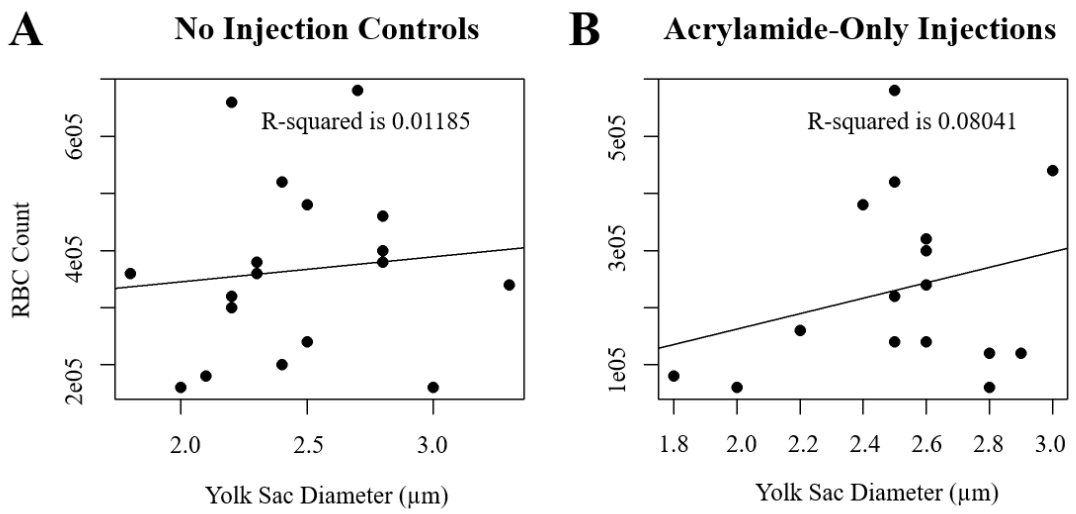


Figure 6. Lack of Correlation Between Red Blood Cell Count and Yolk Sac Diameter. Scatterplots of red blood cell (RBC) counts compared to yolk sac diameter for no injection controls (A) and acrylamide-only injections (B). Adjusted R-squared values indicate no correlation.

# DISCUSSION

This study shows that lowering the hemodynamic load in mouse embryos, through the prevention of red blood cell entry into the circulatory system, results in abnormalities to heart size, myocardial thickness, trabeculation, and looping. Furthermore, acrylamide can result in a reduction of circulating red blood cells (a probable sign of reduced hematocrit) and can also impair some aspects of heart development like trabeculation and looping.

The defects present in low-loaded embryos included a reduction in heart volume size (only present in later stage embryos) and a decrease in myocardial thickness. This corroborates previous findings in chicks where both volume and compact myocardial thickness where reduced in experimentally altered low-loaded left ventricles (Sedmera et al., 1999).

Low-loaded embryos and Ao embryos both resulted in compact trabeculation and more linearized heart tubes. Again, these defects were expected as similar results were shown previously in embryos with reduced hemodynamic loading; however, acrylamide by itself was not expected to affect heart morphology. This led to experiments which assessed the validity the utilized methods by looking at developmental delay in genetically and physically altered embryos.

The effects of acrylamide treatment on heart development begs the question as to why the acrylamide polymerization approach was used in the first place. There are two main reasons to justify this approach. First, injection of acrylamide alone into the blood islands did not impair blood vessel development or somitogenesis (Table 1), so it was not

expected to affect heart development (Lucitti et al., 2007). Second, there was not a better option for a polymerizing agent that can prevent blood cells from entering circulation. Acrylamide is commonly known as a neurotoxin (LoPachin and Gavin, 2012), and while non-toxic gelling agents exist, such as hydrogels (synthesized from poly(vinyl alcohol)), there are still problems that can arise when using them. For example, polymerizing molecules are intrinsically electrophilic. This property allows the molecule to create the necessary covalent bonds needed for gel formation. However, many biological macromolecules are nucleophilic, leading to easy bond formation, and therefore toxicity, with the electrophilic polymerizing molecules (LoPachin and Gavin, 2012). Also, catalyzing the polymerization reaction of non-toxic gels, such as hydrogels, is accomplished through harmful reactants/initiators like formaldehyde, UV-irradiation, and gamma rays (Ahmed, 2015). Therefore, caveats were bound to form no matter what method was chosen.

In this study, it was shown that acrylamide-only injections did not cause developmental delay, but acrylamide and TEMED injections did. To confirm that a lowered hemodynamic load was causing developmental delay and not a synergistic effect of the acrylamide and TEMED acting together, developmental delay was assessed in genetically modified mice that have reduced hemodynamic load through *Myl7* knockout. These mice also exhibited developmental delay and confirmed that the synergistic action of acrylamide and TEMED together was not the cause of developmental delay. It should be noted that the premise of this project was to leave altered genetics out of the study to assess how hemodynamic loading by itself affects development; however, the use of this data helped validate the utilized methods.

While acrylamide by itself might impair heart development in other ways, like direct interaction with the heart or through altered signaling achieved by protein degradation, here it was shown that acrylamide reduced the amount of circulating red blood cells (Table 4). Considering that hematocrit levels determine blood viscosity, and viscosity affects the amount of hemodynamic force (Secomb, 2016), I propose that treatment of acrylamide alone may partly reduce the hemodynamic load. In this way it seems hemodynamic signaling acts in a continuum in its ability to modulate heart develop, where low levels of hemodynamic load (no blood cells in circulation; AT) results in defects of volume size, compact myocardial thickness, trabeculation, and looping, but medium levels of hemodynamic loading (a reduced number of circulating blood cells; Ao) results in trabeculation and looping defects. This correlates with previous studies performed on chick embryos where different amounts of hemodynamic loading, modulated by the extent of conotruncal binding, can lead to different types of CHD (Midgett et al., 2017). Furthermore, Hogers and colleagues showed that decreased hemodynamic loading by vitelline vein ligation still resulted in 36% of the chicks having a normally developed heart (Hogers et al., 1997). In chicken models with low hemodynamic loading through left atrial ligation, the cells of the left ventricle showed decreased proliferation, and diminished myosin immunostaining (decreased contractile function) (Sedmera et al., 2002), but in a study looking at the effect of high hemodynamic loading, there was increased myocardial proliferation (DeAlmeida et al., 2007). These studies indicate that there is a threshold that must be passed for hemodynamic load to affect morphogenesis. Thus, in future studies, it may be interesting to test if increasing the hemodynamic load has an opposite effect on heart development. This could

potentially be done by culturing mouse embryos in erythropoietin, which has been shown to increase hematocrit levels (Mary E. Dickinson, Ph.D., Baylor College of Medicine, personal communication).

There is still much to learn pertaining to how hemodynamics affect heart morphology. For example, hypoplastic left heart syndrome typically forms secondary to aortic stenosis. In contrast, simulating aortic stenosis, via conotruncal binding experiments, results in an opposite phenotype of left ventricular hypertrophy (Sedmera et al., 1999). There is speculation that the longer gestation period in humans is what causes this difference, whereby hypoplastic left heart disease develops as a coping method for the continuous and elongated time that the stress caused by the increased afterload can be inflicted on the human heart during develop (Krishnan et al., 2014). However, in adults that develop aortic stenosis, the heart's coping method does result in left ventricular hypertrophy (Grimard et al., 2016), the condition seen in experimental chick embryos. This data, along with a study done in zebrafish which showed that altered hemodynamic loading only affects heart morphology at a certain time during development (Johnson et al., 2015), indicates that hemodynamic load can act in different ways at different time points. Future studies may need to evaluate time-dependent factors by altering hemodynamic loading in different stage embryos.

Based on this study, decreased hemodynamic loading negatively impacts morphogenesis of the mammalian heart, and if development were to continue, it would likely give rise to a congenital heart defect. In people, low hemodynamic loading could be caused by multiple reasons, but one that is equivalent to this study is anemia (a lack of red blood cells in circulation), which has a high association with CHD (El-Koofy et al.,

2017; Miyamoto et al., 2015). In a recent study, women who supplemented their diet with folic acid —a common treatment for adult anemia because it promotes erythropoiesis— before and during their pregnancy were shown to have a decreased risk of delivering a child with CHD (Mao et al., 2017). Additionally, ethanol-induced CHD in zebrafish embryos can be corrected with the addition of folic acid (Sarmah and Marrs, 2013). In mouse embryos, ethanol was further shown to alter lipid-related gene expression in the heart which was, again, corrected with folic acid (Linask and Han, 2016). Whether or not folic acid aided in altering the hemodynamics of these embryos was not investigated.

As eluded to above, it is likely that a continued low-loading scenario would give rise to a congenital heart defect. Thus, it would be ideal to extend this study past the E9.5 stage of mouse heart development, so that the morphology of other structures that form later (such as septate and valves) could be assessed. However, one caveat is to overcome is the limitations of mouse embryo culture. It is possible that mouse embryos can be manipulated and cultured up until E12.5, but this requires enhanced technical skills, and other pieces of equipment (roller bottles attached to gas line) (Yashiro et al., 2007). Further, embryos cannot currently be cultured past E12.5, but there is an *in vivo* technique called the *exo utero* development system which allows for surgical exposure of the embryos (to allow for experimental manipulations) followed by closure and continued growth within the mother. As this technique is also limited by the presence of the amniotic sack, doing surgical interventions like suturing can still be problematic (Yamada et al., 2008).

In addition to assessing the impact of hemodynamic loading on later staged hearts, another future direction would be to determine the molecular mechanisms by

which the heart responds to hemodynamic load. As mentioned before in the introduction, non-motile cilia have been found to be responsive to shear stress and this signaling is necessary for trabecula development. It is hypothesized that non-motile cilia undergo mechanotransduction because the cilia become deflected with flow, and presumably this causes mechanical stretching and activation of receptors at the membrane (Samsa et al., 2015). Since cilia are gaining prevalence as the main detector of shear stress, these studies on hemodynamic load are gaining more importance as a link to CHD development. In validation of this discovery, defects in cilia development and function have recently been correlated with CHD development in mice through a large-scale mutagenesis screen (Klena et al., 2017) and ciliopathies are heavily associated with heterotaxy which is defined as any condition where heart defects are found simultaneously with other organ defects (Russell et al., 2018). In addition to cilia, evidence from endothelial cells suggest other possible modes of mechanotransduction that may also need to be explored: from stretching of adherens junctions (induced by pressure forces), to activation of ion channels (Haack and Abdelilah-Seyfried, 2016). Therefore, the next step in this process should be to understand how the heart is responding to hemodynamic load on a cellular level.

## REFERENCES


**Ahmed, E. M.** (2015). Hydrogel: Preparation, characterization, and applications: A review. *J. Adv. Res.* **6**, 105–121.

**Anderson, R. H., Brown, N. A. and Moorman, A. F. M.** (2006). Development and structures of the venous pole of the heart. *Dev. Dyn.* **235**, 2–9.

**Anderson, G. A., Udan, R. S., Dickinson, M. E. and Henkelman, R. M.** (2015). Cardiovascular patterning as determined by hemodynamic forces and blood vessel genetics. *PLoS One* **10**, e0137175.

**Arora, R., Trehan, V., Kumar, A., Kalra, G. S. and Nigam, M.** (2003). Transcatheter closure of congenital ventricular septal defects: Experience with various devices. *J. Interv. Cardiol.* **16**, 83–91.

**Arora, R., Trehan, V., Thakur, A. K., Mehta, V., Sengupta, P. P. and Nigam, M.** (2004). Transcatheter closure of congenital muscular ventricular septal defect. *J. Interv. Cardiol.* **17**, 109–115.

**Atkinson, H.** (1973). The respiratory physiology of the marine nematodes Enoplus brevis (Bastian) and E. communis (Bastian). *J. Exp. Biol.* **59**, 255–266.

**Auman, H. J., Coleman, H., Riley, H. E., Olale, F., Tsai, H. J. and Yelon, D.** (2007). Functional modulation of cardiac form through regionally confined cell shape changes. *PLoS Biol.* **5**, e53.

**Ávila, P., Oliver, J. M., Gallego, P., González-García, A., Rodríguez-Puras, M. J., Cambronero, E., Ruiz-Cantador, J., Campos, A., Peinado, R., Prieto, R., et al.** (2017). Natural history and clinical predictors of atrial tachycardia in adults with congenital heart disease. *Circ. Arrhythmia Electrophysiol.* **10**, e005396.

**Axt-Fliedner, R., Kreiselmaier, P., Schwarze, A., Krapp, M. and Gembruch, U.** (2006). Development of hypoplastic left heart syndrome after diagnosis of aortic stenosis in the first trimester by early echocardiography. *Ultrasound Obstet. Gynecol.* **28**, 106–109.

**Balci, A., Sollie-Szarynska, K. M., van der Bijl, A. G. L., Ruys, T. P. E., Mulder, B. J. M., Roos-Hesselink, J. W., van Dijk, A. P. J., Wajon, E. M. C. J., Vliegen, H. W., Drenthen, W., et al.** (2014). Prospective validation and assessment of cardiovascular and offspring risk models for pregnant women with congenital heart disease. *Heart* **100**, 1373–1381.

**Bardo, D. M. E., Frankel, D. G., Applegate, K. E., Murphy, D. J. and Saneto, R. P.** (2001). Hypoplastic left heart syndrome. *RadioGraphics* **21**, 705–717.

**Barik, R.** (2016). Transcatheter closure of post-myocardial infarction ventricular defect: Where are we? *Indian Heart J.* **68**, 99–101.

**Berdougo, E., Coleman, H., Lee, D. H., Stainier, D. Y. R. and Yelon, D.** (2003). Mutation of weak atrium/atrial myosin heavy chain disrupts atrial function and influences ventricular morphogenesis in zebrafish. *Development* **130**, 6121–6129.

**Biben, C. and Harvey, R. P.** (1997). Homeodomain factor Nkx2-5 controls left/right asymmetric expression of bHLH gene eHAND during murine heart development. *Genes Dev.* **11**, 1357–1369.

**Bussmann, J., Bakkers, J. and Schulte-Merker, S.** (2007). Early endocardial morphogenesis requires Scl/Tal1. *PLoS Genet.* **3**, 1425–1437.

**Carroll, K. J., Makarewich, C. A., McAnally, J., Anderson, D. M., Zentilin, L., Liu, N., Giacca, M., Bassel-Duby, R. and Olson, E. N.** (2016). A mouse model for adult cardiac-specific gene deletion with CRISPR/Cas9. *Proc. Natl. Acad. Sci.* **113**, 338–343.

**Chen, H.** (2004). BMP10 is essential for maintaining cardiac growth during murine cardiogenesis. *Development* **131**, 2219–2231.

**Clark, K. L., Yutzey, K. E. and Benson, D. W.** (2006). Transcription factors and congenital heart defects. *Annu. Rev. Physiol.* **68**, 97–121.

**Combs, M. D. and Yutzey, K. E.** (2009). Heart valve development: Regulatory networks in development and disease. *Circ. Res.* **105**, 408–421.

**Curti, A., Lapucci, C., Berto, S., Prandstraller, D., Perolo, A., Rizzo, N. and Farina, A.** (2016). Maternal plasma mRNA species in fetal heart defects: a potential for molecular screening. *Prenat. Diagn.* **36**, 738–743.

**Dai, X.-M., Zong, X.-H., Sylvestre, V. and Stanley, E. R.** (2004). Incomplete restoration of colony-stimulating factor 1 (CSF-1) function in CSF-1–deficient Csf1 op /Csf1 op mice by transgenic expression of cell surface CSF-1. *Blood* **103**, 1114–1123.

**DeAlmeida, A., McQuinn, T. and Sedmera, D.** (2007). Increased ventricular preload is compensated by myocyte proliferation in normal and hypoplastic fetal chick left ventricle. *Circ. Res.* **100**, 1363–1370.

**Devine, W. P., Wythe, J. D., George, M., Koshiba-Takeuchi, K. and Bruneau, B. G.** (2014). Early patterning and specification of cardiac progenitors in gastrulating mesoderm. *Elife* **3**, e03848.

**Digilio, M. C. and Marino, B.** (2016). What is new in genetics of congenital heart defects? *Front. Pediatr.* **4**, 120.

**El-Koofy, N., Mahmoud, A. M. and Fattouh, A. M.** (2017). Nutritional rehabilitation for children with congenital heart disease with left to right shunt. *Turk. J. Pediatr.* **59**, 442–451.

**Fananapazir, K. and Kaufman, M. H.** (1988). Observations on the development of the aortico-pulmonary spiral septum in the mouse. *J. Anat.* **158**, 157–72.

**Ferdous, A., Caprioli, A., Iacovino, M., Martin, C. M., Morris, J., Richardson, J. A., Latif, S., Hammer, R. E., Harvey, R. P., Olson, E. N., et al.** (2009). Nkx2-5 transactivates the Ets-related protein 71 gene and specifies an endothelial/endocardial fate in the developing embryo. *Proc. Natl. Acad. Sci.* **106**, 814–819.

**Freud, L. R., McElhinney, D. B., Marshall, A. C., Marx, G. R., Friedman, K. G., del Nido, P. J., Emani, S. M., Lafranchi, T., Silva, V., Wilkins-Haug, L. E., et al.** (2014). Fetal aortic valvuloplasty for evolving hypoplastic left heart syndrome: postnatal outcomes of the first 100 patients. *Circulation* **130**, 638–645.

**Gassmann, M., Casagranda, F., Orloli, D., Simon, H., Lai, C., Kleint, R. and Lemke, G.** (1995). Aberrant neural and cardiac development in mice lacking the ErbB4 neuregulin receptor. *Nature* **378**, 390–394.

**Ghorbel, I., Maktouf, S., Kallel, C., Ellouze Chaabouni, S., Boudawara, T. and Zeghal, N.** (2015). Disruption of erythrocyte antioxidant defense system, hematological parameters, induction of pro-inflammatory cytokines and DNA damage in liver of co-exposed rats to aluminium and acrylamide. *Chem. Biol. Interact.* **236**, 31–40.

**Gianicolo, E. A. L., Cresci, M., Ait-Ali, L., Foffa, I. and Andreassi, M. G.** (2010). Smoking and congenital heart disease: the epidemiological and biological link. *Curr. Pharm. Des.* **16**, 2572–7.

**Gilboa, S. M., Salemi, J. L., Nembhard, W. N., Fixler, D. E. and Correa, A.** (2010). Children and adults in the United States, 1999 to 2006. **122**, 2254–2263.

**Goo, S., Joshi, P., Sands, G., Gerneke, D., Taberner, A., Dollie, Q., LeGrice, I. and Loiselle, D.** (2009). Trabeculae carneae as models of the ventricular walls: implications for the delivery of oxygen. *J. Gen. Physiol.* **134**, 339–350.

**Gorini, F., Chiappa, E., Gargani, L. and Picano, E.** (2014). Potential effects of environmental chemical contamination in congenital heart disease. *Pediatr. Cardiol.* **35**, 559–568.

**Granados-Riveron, J. T. and Brook, J. D.** (2012). The impact of mechanical forces in heart morphogenesis. *Circ. Cardiovasc. Genet.* **5**, 132–142.

**Grego-Bessa, J., Luna-Zurita, L., del Monte, G., Bolós, V., Melgar, P., Arandilla, A., Garratt, A. N., Zang, H., Mukouyama, Y. suke, Chen, H., et al.** (2007). Notch signaling is essential for ventricular chamber development. *Dev. Cell* **12**, 415–429.

**Greutmann, M. and Tobler, D.** (2012). Changing epidemiology and mortality in adult congenital heart disease: looking into the future. *Future Cardiol.* **8**, 171–177.

**Grimard, B. H., Safford, R. E. and Burns, E. L.** (2016). Aortic stenosis: Diagnosis and treatment. *Am. Fam. Physician* **93**, 371–378.

**Groenendijk, B. C. W., Van der Heiden, K., Hierck, B. P. and Poelmann, R. E.** (2007). The role of shear stress on ET-1, KLF2, and NOS-3 expression in the developing cardiovascular system of chicken embryos in a venous ligation model. *Physiology (Bethesda).* **22**, 380–389.

**Haack, T. and Abdelilah-Seyfried, S.** (2016). The force within: endocardial development, mechanotransduction and signalling during cardiac morphogenesis. *Development* **143**, 373–386.

**Hahn, C. and Schwartz, M. A.** (2009). Mechanotransduction in vascular physiology and atherogenesis. *Nat. Rev. Mol. Cell Biol.* **10**, 53–62.

**Hoffman, J. I.** (1995). Incidence of congenital heart disease: II. Prenatal incidence. *Pediatr Cardiol.* **16**, 155–165.

**Hoffman, J. I. E. and Kaplan, S.** (2002). The incidence of congenital heart disease. *J. Am. Coll. Cardiol.* **39**, 1890–1900.

**Hogers, B., DeRuiter, M. C., Gittenberger-de Groot, A. C. and Poelmann, R. E.** (1997). Unilateral vitelline vein ligation alters intracardiac blood flow patterns and morphogenesis in the chick embryo. *Circ. Res.* **80**, 473–481.

**Hove, J. R., Köster, R. W., Forouhar, A. S., Acevedo-Bolton, G., Fraser, S. E. and Gharib, M.** (2003). Intracardiac fluid forces are an essential epigenetic factor for embryonic cardiogenesis. *Nature* **421**, 172–177.

**Huang, C.** (2003). Embryonic atrial function is essential for mouse embryogenesis, cardiac morphogenesis and angiogenesis. *Development* **130**, 6111–6119.

**Hughes, C. J. R. and Jacobs, J. R.** (2017). Dissecting the role of the extracellular matrix in heart disease: Lessons from the Drosophila genetic model. *Vet. Sci.* **4**, 24.

**Iacobazzi, D., Suleiman, M. S., Ghorbel, M., George, S. J., Caputo, M. and Tulloh, R. M.** (2016). Cellular and molecular basis of RV hypertrophy in congenital heart disease. *Heart* **102**, 12–17.

**Iomini, C., Tejada, K., Mo, W., Vaananen, H. and Piperno, G.** (2004). Primary cilia of human endothelial cells disassemble under laminar shear stress. *J. Cell Biol.* **164**, 811–817.

**Ivanovitch, K., Esteban, I. and Torres, M.** (2017). Growth and morphogenesis during early heart development in amniotes. *J. Cardiovasc. Dev. Dis.* **4**, 20.

**Jenkins, K. J., Correa, A., Feinstein, J. A., Botto, L., Britt, A. E., Daniels, S. R., Elixson, M., Warnes, C. A. and Webb, C. L.** (2007). Noninherited risk factors and congenital cardiovascular defects: Current knowledge - A scientific statement from the American Heart Association Council on Cardiovascular Disease in the Young. *Circulation* **115**, 2995–3014.

**Jiang, L., Zhu, H.-Z., Xu, Y.-Z., Ni, J.-Z., Zhang, Y. and Liu, Q.** (2013). Comparative selenoproteome analysis reveals a reduced utilization of selenium in parasitic platyhelminthes. *PeerJ* **1**, e202.

**Johnson, B., Bark, D., Van Herck, I., Garrity, D. and Dasi, L. P.** (2015). Altered mechanical state in the embryonic heart results in time-dependent decreases in cardiac function. *Biomech. Model. Mechanobiol.* **14**, 1379–1389.

**Karunamuni, G., Gu, S., Doughman, Y. Q., Peterson, L. M., Mai, K., McHale, Q., Jenkins, M. W., Linask, K. K., Rollins, A. M. and Watanabe, M.** (2014). Ethanol exposure alters early cardiac function in the looping heart: a mechanism for congenital heart defects? *AJP Hear. Circ. Physiol.* **306**, H414–H421.

**Kaufman, M. and Bard, J.** (1999). *The Anatomical Basis of Mouse Development*. 1st ed. San Diego: Academic Press.

**Kaufman, M. H. and Navaratnam, V.** (1981). Early differentiation of the heart in mouse embryos. *J. Anat.* **133**, 235–246.

**Keegan, B. R., Meyer, D. and Yelon, D.** (2004). Organization of cardiac chamber progenitors in the zebrafish blastula. *Development* **131**, 3081–3091.

**Kelly, R. G., Buckingham, M. E. and Moorman, A. F.** (2014). Heart fields and cardiac morphogenesis. *Cold Spring Harb. Perspect. Med.* **4**, a015750.

**Khairy, P., Ionescu-Ittu, R., MacKie, A. S., Abrahamowicz, M., Pilote, L. and Marelli, A. J.** (2010). Changing mortality in congenital heart disease. *J. Am. Coll. Cardiol.* **56**, 1149–1157.

**Klena, N. T., Gibbs, B. C. and Lo, C. W.** (2017). Cilia and ciliopathies in congenital heart disease. *Cold Spring Harb. Perspect. Biol.* **9**, a028266.

**Krishnan, A., Samtani, R., Dhanantwari, P., Lee, E., Yamada, S., Shiota, K., Donofrio, M. T., Leatherbury, L. and Lo, C. W.** (2014). A detailed comparison of mouse and human cardiac development. *Pediatr. Res.* **76**, 500–507.

**Lage, K., Greenway, S. C., Rosenfeld, J. A., Wakimoto, H., Gorham, J. M., Segre, A. V., Roberts, A. E., Smoot, L. B., Pu, W. T., C. Pereira, A., et al.** (2012). Genetic and environmental risk factors in congenital heart disease functionally converge in protein networks driving heart development. *Proc. Natl. Acad. Sci.* **109**, 14035–14040.

**Le Garrec, J. F., Domínguez, J. N., Desgrange, A., Ivanovitch, K. D., Raphaël, E., Bangham, J. A., Torres, M., Coen, E., Mohun, T. J. and Meilhac, S. M.** (2017). A predictive model of asymmetric morphogenesis from 3D reconstructions of mouse heart looping dynamics. *Elife* **6**, e28951.

**Lee, K. F., Simon, H., Chen, H., Bates, B., Hung, M. C. and Hauser, C.** (1995). Requirement for neuregulin receptor erbB2 in neural and cardiac development. *Nature* **378**, 394–398.

**Linask, K. K. and Han, M.** (2016). Acute alcohol exposure during mouse gastrulation alters lipid metabolism in placental and heart development: Folate prevention. *Birth Defects Res. Part A - Clin. Mol. Teratol.* **106**, 749–760.

**Linask, K. K., Han, M. Da, Linask, K. L., Schlange, T. and Brand, T.** (2003). Effects of antisense misexpression of CFC on downstream flectin protein expression during heart looping. *Dev. Dyn.* **228**, 217–230.

**Linask, K. K., Han, M., Cai, D. H., Brauer, P. R. and Maisastry, S. M.** (2005). Cardiac morphogenesis: Matrix metalloproteinase coordination of cellular mechanisms underlying heart tube formation and directionality of looping. *Dev. Dyn.* **233**, 739–753.

**Lints, T. J., Parsons, L. M., Hartley, L., Lyons, I. and Harvey, R. P.** (1993). Nkx-2.5: a novel murine homeobox gene expressed in early heart progenitor cells and their myogenic descendants. *Development* **119**, 419–431.

**Liu, J., Bressan, M., Hassel, D., Huisken, J., Staudt, D., Kikuchi, K., Poss, K. D., Mikawa, T. and Stainier, D. Y. R.** (2010). A dual role for ErbB2 signaling in cardiac trabeculation. *Development* **137**, 3867–3875.

**LoPachin, R. M. and Gavin, T.** (2012). Molecular mechanism of acrylamide neurotoxicity: Lessons learned from organic chemistry. *Environ. Health Perspect.* **120**, 1650–1657.

**Lucitti, J. L., Jones, E. A. V., Huang, C., Chen, J., Fraser, S. E. and Dickinson, M. E.** (2007). Vascular remodeling of the mouse yolk sac requires hemodynamic force. *Development* **134**, 3317–3326.

**Lyons, I., Parsons, L. M., Hartley, L., Li, R., Andrews, J. E., Robb, L. and Harvey, R. P.** (1995). Myogenic and morphogenetic defects in the heart tubes of murine embryos lacking the homeo box gene Nkx2-5. *Genes Dev.* **9**, 1654–1666.

**Mahler, G. J. and Butcher, J. T.** (2011). Cardiac developmental toxicity. *Birth Defects Res. Part C - Embryo Today Rev.* **93**, 291–297.

**Makwana, O., King, N. M. P., Ahles, L., Selmin, O., Granzier, H. L. and Runyan, R. B.** (2010). Exposure to low-dose trichloroethylene alters shear stress gene expression and function in the developing chick heart. *Cardiovasc. Toxicol.* **10**, 100–107.

**Männer, J.** (2009). The anatomy of cardiac looping: A step towards the understanding of the morphogenesis of several forms of congenital cardiac malformations. *Clin. Anat.* **22**, 21–35.

**Mao, B., Qiu, J., Zhao, N., Shao, Y., Dai, W., He, X., Cui, H., Lin, X., Lv, L., Tang, Z., et al.** (2017). Maternal folic acid supplementation and dietary folate intake and congenital heart defects. *PLoS One* **12**, 187996.

**Marelli, A. J., Mackie, A. S., Ionescu-Ittu, R., Rahme, E. and Pilote, L.** (2007). Congenital heart disease in the general population: Changing prevalence and age distribution. *Circulation* **115**, 163–172.

**Markwald, R. R., Fitzharris, T. P. and Manasek, F. J.** (1977). Structural development of endocardial cushions. *Am. J. Anat.* **148**, 85–119.

**May, S. R., Stewart, N. J., Chang, W. and Peterson, A. S.** (2004). A Titin mutation defines roles for circulation in endothelial morphogenesis. *Dev. Biol.* **270**, 31–46.

**McElhinney, D. B., Marshall, A. C., Wilkins-Haug, L. E., Brown, D. W., Benson, C. B., Silva, V., Marx, G. R., Mizrahi-Arnaud, A., Lock, J. E. and Tworetzky, W.** (2009). Predictors of technical success and postnatal biventricular outcome after in utero aortic valvuloplasty for aortic stenosis with evolving hypoplastic left heart syndrome. *Circulation* **120**, 1482–1490.

**Meyer, D. and Birchmeier, C.** (1995). Multiple essential functions of neuregulin in development. *Nature* **378**, 386–390.

**Midgett, M. and Rugonyi, S.** (2014). Congenital heart malformations induced by hemodynamic altering surgical interventions. *Front. Physiol.* **5 JUL**, 1–18.

**Midgett, M., Thornburg, K. and Rugonyi, S.** (2017). Blood flow patterns underlie developmental heart defects. *Am. J. Physiol. - Hear. Circ. Physiol.* **312**, H632–H642.

**Milgrom-Hoffman, M., Harrelson, Z., Ferrara, N., Zelzer, E., Evans, S. M. and Tzahor, E.** (2011). The heart endocardium is derived from vascular endothelial progenitors. *Development* **138**, 4777–4787.

**Minette, M. S. and Sahn, D. J.** (2006). Ventricular septal defects. *Circulation* **114**, 2190–2197.

**Misfeldt, A. M., Boyle, S. C., Tompkins, K. L., Bautch, V. L., Labosky, P. A. and Baldwin, H. S.** (2009). Endocardial cells are a distinct endothelial lineage derived from Flk1+ multipotent cardiovascular progenitors. *Dev. Biol.* **333**, 78–89.

**Mitchell, S. C., Korones, S. B. and Berendes, H. W.** (1971). Congenital heart disease in 56,109 births. Incidence and natural history. *Circulation* **43**, 323–332.

**Miyamoto, K., Inai, K., Takeuchi, D., Shinohara, T. and Nakanishi, T.** (2015). Relationships among red cell distribution width, anemia, and interleukin-6 in adult congenital heart disease. *Circ. J.* **79**, 1100–1106.

**Morris, J. K., Weichun, L., Hauser, C., Marchuk, Y., Getman, D. and Kuo-Fen, L.** (1999). Rescue of the cardiac defect in erbB2 mutant mice reveals essential roles of erbB2 in peripheral nervous system development. *Neuron* **23**, 273–283.

**Nandi, D., Rossano, J. W., Wang, Y. and Jerrell, J. M.** (2017). Risk factors for heart failure and its costs among children with complex congenital heart disease in a medicaid cohort. *Pediatr. Cardiol.* **38**, 1672–1679.

**Nelle, M., Raio, L., Pavlovic, M., Carrel, T., Surbek, D. and Meyer-Wittkopf, M.** (2009). Prenatal diagnosis and treatment planning of congenital heart defects—possibilities and limits. *World J. Pediatr.* **5**, 18–22.

**Norwood WI, Lang P, H. D.** (1983). Physiologic repair of aortic atresia-hypoplastic left heart syndrome. | Harvard Catalyst Profiles | Harvard Catalyst. *N Engl J Med.* **308**, 23–6.

**Palencia-Desai, S., Rost, M. S., Schumacher, J. A., Ton, Q. V., Craig, M. P., Baltrunaite, K., Koenig, A. L., Wang, J., Poss, K. D., Chi, N. C., et al.** (2015).

Myocardium and BMP signaling are required for endocardial differentiation. *Development* **142**, 2304–2315.

**Palis, J.** (2014). Primitive and definitive erythropoiesis in mammals. *Front. Physiol.* **5**, 1–9.

**Parrie, L. E., Renfrew, E. M., Wal, A. Vander, Mueller, R. L. and Garrity, D. M.** (2013). Zebrafish tbx5 paralogs demonstrate independent essential requirements in cardiac and pectoral fin development. *Dev. Dyn.* **242**, 485–402.

**Pashmforoush, M., Lu, J. T., Chen, H., St. Amand, T., Kondo, R., Pradervand, S., Evans, S. M., Clark, B., Feramisco, J. R., Giles, W., et al.** (2004). Nkx2-5 pathways and congenital heart disease: Loss of ventricular myocyte lineage specification leads to progressive cardiomyopathy and complete heart block. *Cell* **117**, 373–386.

**Person, A. D., Klewer, S. E. and Runyan, R. B.** (2005). Cell biology of cardiac cushion development. *Int. Rev. Cytol.* **243**, 287–335.

**Peshkovsky, C., Totong, R. and Yelon, D.** (2011). Dependence of cardiac trabeculation on neuregulin signaling and blood flow in zebrafish. *Dev. Dyn.* **240**, 446–456.

**Piao, L., Fang, Y. H., Cadete, V. J. J., Wietholt, C., Urboniene, D., Toth, P. T., Marsboom, G., Zhang, H. J., Haber, I., Rehman, J., et al.** (2010). The inhibition of pyruvate dehydrogenase kinase improves impaired cardiac function and electrical remodeling in two models of right ventricular hypertrophy: Resuscitating the hibernating right ventricle. *J. Mol. Med.* **88**, 47–60.

**Pittman, R. N.** (2016). *Regulation of Tissue Oxygenation*. 2nd ed. (ed. Granger, D. N.) and Granger, J. P.).

**Prendiville, T., Jay, P. Y. and Pu, W. T.** (2014). Insights into the genetic structure of congenital heart disease from human and murine studies on monogenic disorders. *Cold Spring Harb. Perspect. Med.* **4**, 1–14.

**Qipshidze, N., Tyagi, N., Metreveli, N., Lominadze, D. and Tyagi, S. C.** (2012). Autophagy mechanism of right ventricular remodeling in murine model of pulmonary artery constriction. *Am. J. Physiol. Circ. Physiol.* **302**, H688–H696.

**Rufer, E. S., Hacker, T. A., Flentke, G. R., Drake, V. J., Brody, M. J., Lough, J. and Smith, S. M.** (2009). Altered cardiac function and ventricular septal defect in avian embryos exposed to low-dose trichloroethylene. *Toxicol. Sci.* **113**, 444–452.

**Russell, M. W., Chung, W. K., Kaltman, J. R. and Miller, T. A.** (2018). Advances in the Understanding of the Genetic Determinants of Congenital Heart Disease and Their Impact on Clinical Outcomes. *J. Am. Heart Assoc.* **7**.

**Samsa, L. A., Givens, C., Tzima, E., Stainier, D. Y. R., Qian, L. and Liu, J.** (2015). Cardiac contraction activates endocardial Notch signaling to modulate chamber maturation in zebrafish. *Development* **142**, 4080–4091.

**Sarmah, S. and Marrs, J. A.** (2013). Complex cardiac defects after ethanol exposure during discrete cardiogenic events in zebrafish: Prevention with folic acid. *Dev. Dyn.* **242**, 1184–1201.

**Savolainen, S. M., Foley, J. F. and Elmore, S. A.** (2009). Histology atlas of the developing mouse heart with emphasis on E11.5 to E18.5. *Toxicol. Pathol.* **37**, 395–414.

**Schott, J., DW, B., CT, B., W, P., GM, S., JP, M., BJ, M., CE, S. and JG, S.** (1998). Congenital heart disease caused by mutations in the transcription factor NKX2-5. *Science.* **281**, 108–111.

**Seal, R.** (2011). Adult congenital heart disease. *Paediatr. Anaesth.* **21**, 615–622.

**Secomb, T. W.** (2016). Hemodynamics. *Compr. Physiol.* **6**, 975–1003.

**Sedmera, D., Pexieder, T., Rychterova, V., Hu, N. and Clark, E. B.** (1999). Remodeling of chick embryonic ventricular myoarchitecture under experimentally changed loading conditions. *Anat. Rec.* **254**, 238–252.

**Sedmera, D., Pexieder, T., Vuillemin, M., Thompson, R. P. and Anderson, R. H.** (2000). Developmental patterning of the myocardium. *Anat. Rec.* **258**, 319–337.

**Sedmera, D., Hu, N., Weiss, K. M., Keller, B. B., Denslow, S. and Thompson, R. P.** (2002). Cellular changes in experimental left heart hypoplasia. *Anat. Rec.* **267**, 137–145.

**Shi, J., Zhao, W., Pan, B., Zheng, M., Si, L., Zhu, J., Liu, L. and Tian, J.** (2017). Alcohol exposure causes overexpression of heart development-related genes by affecting the histone H3 acetylation via BMP signaling pathway in cardiomyoblast cells. *Alcohol. Clin. Exp. Res.* **41**, 87–95.

**Singh, M., Nair, A., Vadakkan, T., Piazza, V., Udan, R., Frazier, M. V., Janecek, T., Dickinson, M. E. and Larin, K. V.** (2015). Comparison of optical projection tomography and optical coherence tomography for assessment of murine embryonic development. *SPIE BiOS* **9334**.

**Smoak, I. W.** (2002). Hypoglycemia and embryonic heart development. *Front. Biosci.* **7**, 307–318.

**Srivastava, D., Thomas, T., Lin, Q., Kirby, M. L., Brown, D. and Olson, E. N.** (1997). Regulation of cardiac mesodermal and neural crest development by the bHLH transcription factor, dHAND. *Nat. Genet.* **16**, 154–160.

**Staudt, D. W., Liu, J., Thorn, K. S., Stuurman, N., Liebling, M. and Stainier, D. Y. R.** (2014). High-resolution imaging of cardiomyocyte behavior reveals two distinct steps in ventricular trabeculation. *Development* **141**, 585–593.

**Tam, P. P., Parameswaran, M., Kinder, S. J. and Weinberger, R. P.** (1997). The allocation of epiblast cells to the embryonic heart and other mesodermal lineages: the role of ingression and tissue movement during gastrulation. *Development* **124**, 1631–1642.

**Tanaka, M., Chen, Z., Bartunkova, S., Yamasaki, N. and Izumo, S.** (1999). The cardiac homeobox gene Csx/Nkx2.5 lies genetically upstream of multiple genes essential for heart development. *Development* **126**, 1269–1280.

**Thakkar, A. N., Chinnadurai, P. and Huie Lin, C.** (2017). Adult congenital heart disease: Magnitude of the problem. *Curr. Opin. Cardiol.* **32**, 467–474.

**Tsuda, T., Philp, N., Zile, M. H. and Linask, K. K.** (1996). Left-right asymmetric localisation of Flectin in the E.C.M. during heart looping. **173**, 39–50.

**Tworetzky, W., Wilkins-Haug, L., Jennings, R. W., Van Der Velde, M. E., Marshall, A. C., Marx, G. R., Colan, S. D., Benson, C. B., Lock, J. E. and Perry, S. B.** (2004). Balloon dilation of severe aortic stenosis in the fetus: Potential for prevention of hypoplastic left heart syndrome. Candidate selection, technique, and results of successful intervention. *Circulation* **110**, 2125–2131.

**Urencio, M., Greenleaf, C., Salazar, J. and Dodge-Khatami, A.** (2016). Resource and cost considerations in treating hypoplastic left heart syndrome. *Pediatr. Heal. Med. Ther.* **Volume 7**, 149–153.

**Vermot, J., Forouhar, A. S., Liebling, M., Wu, D., Plummer, D., Gharib, M. and Fraser, S. E.** (2009). Reversing blood flows act through klf2a to ensure normal valvulogenesis in the developing heart. *PLoS Biol.* **7**.

**Vitarelli, A. and Capotosto, L.** (2011). Role of echocardiography in the assessment and management of adult congenital heart disease in pregnancy. *Int. J. Cardiovasc. Imaging* **27**, 843–857.

**Vogel, T. M. and McCarty, P. L.** (1985). Biotransformation of tetrachloroethylene to trichloroethylene, dichloroethylene, vinyl chloride, and carbon dioxide under methanogenic conditions. *Appl. Environ. Microbiol.* **49**, 1080–1083.

**Wang, D. Z., Reiter, R. S., Lin, J. L., Wang, Q., Williams, H. S., Krob, S. L., Schultheiss, T. M., Evans, S. and Lin, J. J.** (1999). Requirement of a novel gene, Xin, in cardiac morphogenesis. *Development* **126**, 1281–94.

**Wang, C., Xie, L., Zhou, K., Zhan, Y., Li, Y., Li, H., Qiao, L., Wang, F. and Hua, Y.** (2013). Increased risk for congenital heart defects in children carrying the ABCB1 gene C3435T polymorphism and maternal periconceptional toxicants exposure. *PLoS One* **8**.

**Wang, W., Niu, Z., Wang, Y., Li, Y., Zou, H., Yang, L., Meng, M., Wei, C., Li, Q., Duan, L., et al.** (2016). Comparative transcriptome analysis of atrial septal defect identifies dysregulated genes during heart septum morphogenesis. *Gene* **575**, 303–312.

**Wehman, B., Siddiqui, O. T., Mishra, R., Sharma, S. and Kaushal, S.** (2015). Stem cell therapy for CHD: Towards translation. *Cardiol. Young* **25**, 58–66.

**Weissgerber, P., Held, B., Bloch, W., Kaestner, L., Chien, K. R., Fleischmann, B. K., Lipp, P., Flockerzi, V. and Freichel, M.** (2006). Reduced cardiac L-type Ca2+ current in Cav(V)beta2-/- embryos impairs cardiac development and contraction with secondary defects in vascular maturation. *Circ. Res.* **99**, 749–757.

**Wong, K. S., Rehn, K., Palencia-Desai, S., Kohli, V., Hunter, W., Uhl, J. D., Rost, M. S. and Sumanas, S.** (2012). Hedgehog signaling is required for differentiation of endocardial progenitors in zebrafish. *Dev. Biol.* **361**, 377–391.

**Yamada, M., Hatta, T. and Otani, H.** (2008). Mouse exo utero development system: Protocol and troubleshooting. *Congenit. Anom. (Kyoto).* **48**, 183–187.

**Yashiro, K., Shiratori, H. and Hamada, H.** (2007). Haemodynamics determined by a genetic programme govern asymmetric development of the aortic arch. *Nature* **450**, 285–288.

**Yener, Y.** (2013). Effects of long term low dose acrylamide exposure on rat bone marrow polychromatic erythrocytes. *Biotech Histochem* **88**, 356–360.